Green Chemistry

PAPER

View Article Online
View Journal

Cite this: DOI: 10.1039/d6gc00337k

PHA biocomposites from lignocellulose: scalability and sustainability analyses through dynamic simulation, LCA, and TEA

Jhuma Sadhukhan, *[a] Xiaoyan Hu, [a] Ritam Sen, [a] James Bowbrick Smith, [a] Kathleen Dunbar, [a] Angela Bywater,[a] Jeong Jae Wie, [b,c] Chang Geun Yoo [d] and Arthur Ragauskas [e,f]

Lignocellulosic residues are underutilized carbon resources for circular, inherently carbon-negative biopolymer manufacturing. This study presents the first integrated dynamic simulation, life cycle assessment, and techno-economic analysis (DS–LCA–TEA) of polyhydroxyalkanoate (PHA) biocomposite production from lignocellulose. A kinetic and mass transfer-based bioreactor model was developed and calibrated using experimental data for *Cupriavidus necator* cultivated on lignocellulose-derived sugars, reproducing transient biomass and intracellular PHA accumulation (0.55 w/w PHA/substrate and 0.67 w/w PHA per cell dry weight). Dynamic outputs informed plant-wide mass and energy balances for a PHA-biocomposite process, integrating biomass pretreatment, fermentation, natural deep eutectic solvent-based PHA recovery, fiber-PHA compounding, and end-of-life circularity. The LCA results show a global warming potential (GWP) of 1.51 kg CO_2e per kg PHA. Displacing fossil-derived polypropylene yields an estimated 2.18 kg CO_2e per kg or 60% reduction in GWP, with global potential savings of ~340 million tonnes CO_2e per y under 2030 polypropylene demand. Monte Carlo uncertainty analysis confirms a low probability (<4%) of exceeding the GWP of fossil-based-equivalent polypropylene. TEA shows the PHA biocomposite production cost of $2.6 per kg and an economic margin of $4.4 per kg for a production capacity of 1 ktpa. The discounted cash flow analysis shows a production capacity of at least 0.3 ktpa PHA biocomposite for an acceptable payback of <10 years. This work establishes lignocellulosic PHA biocomposites as a scalable, climate-friendly platform material and highlights the centrality of process integration to achieve economic feasibility.

Received 18th January 2026,
Accepted 7th May 2026

DOI: 10.1039/d6gc00337k

rsc.li/greenchem

Green foundation

1. This paper advances green chemistry through valorizing lignocellulosic residues, preventing waste, circularizing resources, and displacing fossil-based single-use plastics, with safer, high-value biodegradable and biocompatible biomaterials. Safer (less toxic) natural resources, such as natural deep eutectic solvents and microbial culture, are utilized. Moderate operating conditions deploy safer chemistry.

2. The study demonstrates quantitatively that lignocellulosic biocomposites achieve 60% GWP reduction, displacing fossil-based polypropylene at competitive costs (€2.2 per kg biocomposites). In-process energy recovery enables a highly resource- and energy-efficient integrated plant. Microbial fermentation replaces hazardous petrochemical polymerization.

3. Further greening could be achieved by integrating CO_2-based fermentation. Additionally, in-process energy/material recovery can be deployed. Biocomposites are durable and renewable, offering long-term carbon storage. A wider range of organic waste resources can be explored to eco-manufacture high-value biomaterials, advancing atom economy.

[a]*University of Surrey, Guildford, GU2 7XH, UK. E-mail: j.sadhukhan@surrey.ac.uk, jhumasadhukhan@gmail.com*
[b]*Department of Organic and Nano Engineering, Hanyang University, 222 Wangsimni-ro, Seongdong-gu, Seoul 04763, Republic of Korea*
[c]*Human-Tech Convergence Program, Hanyang University, 222 Wangsimni-ro, Seongdong-gu, Seoul 04763, Republic of Korea*
[d]*Department of Chemical Engineering, State University of New York College of Environmental Science and Forestry, Syracuse, NY 13210, USA*
[e]*Oak Ridge National Laboratory, 1 Bethel Valley Road, Oak Ridge, TN 37830, USA*
[f]*Department of Chemical and Biomolecular Engineering, The University of Tennessee, 419 Dougherty Engineering Building, 1512 Middle Drive, Knoxville, TN 37996, USA*

Introduction

Global plastic production is projected to increase from 400 million tonnes to 700 million tonnes by 2040,[1] with a market size from ~US$524.5 billion to US$754.2 billion by 2032.[2] Approximately 98% of plastics are petroleum-based, and 99% of petroleum-based plastics are non-biodegradable (Houssini *et al.*, 2025).[3] They, including microplastics, accumulate in freshwater and marine systems, as well as in landfills, posing a threat to ecosystem health. Emissions from fossil fuels used for plastic production must be reduced to mitigate the impact of climate change (BBIA, 2025).[4] Climate impact due to fossil resource deployment is also accelerating at an alarming rate. Emissions peaking by 2025 must fall by 43% by 2030 to remain within that limit (IPCC, 2022).[5] The COP29 advanced the path by agreeing to a new climate finance goal, tripling contributions from developed countries to US$300 billion by 2035, alongside a projected US$1 trillion annually from broader sources (UNCTAD, 2024).[6] As this momentum builds, carbon-neutral bio-based systems that enable greenhouse gas (GHG) emission reduction and material circularity must be focused on.

Emerging carbon utilization and long-term carbon storage strategies offer compelling dual benefits: mitigating GHG emissions and creating circular economies. Polyhydroxyalkanoates (PHAs), a group of polyesters available from waste lignocellulosic biomass resources such as corn and maize stover, wheat and rice straw, sugarcane bagasse and molasses, and sugar beet molasses, are renewable alternatives to fossil-based single-use plastics, mitigating GHG emissions and creating circular economies. PHA-based biocomposites are durable and renewable, offering long-term carbon storage. They, if disposed of in the environment, also readily and completely biodegrade into carbon dioxide, which is sequestered in biomass, closing the carbon cycle. Locking away carbon is the environmental driver in targeting biocomposite production for a variety of added-value products in food, medical, clothing, homecare, healthcare, personal care, transport and agriculture sectors, positioning PHA biocomposite synthesis not just as a substitute for fossil-based plastics, but as an active climate mitigation strategy. In the biomedical sector, its applications are wide-ranging, including implants, cardiovascular grafting, replacing damaged cells, scaffolds for tissue engineering, tissue-engineered heart valves, human embryonic stem cells, cancer therapy, drug delivery, orthopaedics, wound healing, skin repair, *etc*. Microbial intracellular PHA copolymers are inherently biocompatible and biobased. They offer a route to circular, low-emission material synthesis, which is aligned with climate and resource equity goals. Biocomposites are made by reinforcing natural fibers into PHA copolymer matrices. Several companies are already piloting PHAs in compostable packaging, often blended with natural fibers to improve performance while maintaining biodegradability. Thus, PHAs have emerged as a pillar of net-zero circular bioeconomy strategies.

PHAs are a group of molecules with varying chain lengths, short chain length (SCL) comprising 3–5 carbon monomers, such as poly(3-hydroxybutyrate) (PHB), poly(3-hydroxyvalerate) and their copolymer poly(3-hydroxybutyrate-*co*-3-hydroxyvalerate), *etc*., medium chain length comprising 6–14 carbon monomers, such as poly(3-hydroxyoctanoate) and poly(3-hydroxynonanoate), *etc*. (Li *et al.*, 2016),[7] and long chain length with more than 14 carbon atoms, *e.g.*, poly(3-hydroxyoctadecanoate) (Mathuriya and Yakhmi, 2017).[8] SCL PHAs are more amorphous or less crystalline than higher-chain PHAs.

Living cells naturally store carbon and energy in the form of PHAs, which are biodegradable and biocompatible biopolymers, under starvation or famine conditions. Thus, the feast-famine cycle in a sequential reactor configuration supports cellular growth (cultivation) and intracellular PHA accumulation, respectively. There are two ways to feed microorganisms with carbon sources during the cultivation stage. The most common method is using glucose, fructose, or sugars and oily substrates, commonly known as heterotrophic fermentation/cultivation (HF).[9–11] Autotrophic fermentation (AF) is another kind, where carbon dioxide is used as a source of carbon for microbial PHA synthesis.[12–14] In HF, volatile fatty acids, such as acetic acid, generated *via* microbial electrosynthesis of carbon dioxide (*i.e.*, *via* AF) or directly from wastewaters (HF),[15–17] can also be fed to grow microorganisms. There are some other upstream processes to PHA biosynthesis evaluated in the literature, such as sludge pyrolysis followed by volatile fatty acid fermentation, and gasification followed by syngas fermentation,[18] and acidogenic fermentation of organic matter of municipal solid waste (MSW) followed by photobioreduction.[19] *C. necator*, a Gram-negative bacterium commonly isolated from soil and freshwater, is widely known to support both HF and AF and can accumulate PHA up to 90% of cell dry weight (cdw)[20,21] to store carbon and energy. Some studies prefer mixed culture over a particular strain, which is easier to scale up with greater cost-effectiveness. Dias *et al.* (2005) showed a PHA content of up to 78.5% (g g^{-1} volatile suspended solids) of cdw with a mixed culture.[22]

The only pilot study found in the literature applies mixed culture in Biomass Energy Technology Co., Ltd in Zhenjiang, Jiangsu province, China, processing food waste (400 L per ten days without dilution) from Zhenjiang city.[23] The process comprises VFA fermentation, mixed culture enrichment (aerobic feast and famine regime), and PHA accumulation in one scenario, and a rapid biomass proliferation stage embedded after the biomass enrichment stage in a second optimal scenario. Most companies continue to rely on crops, undermining the climate benefits that bioplastics offer. Formerly Danimer Scientific, now Techor Apex (US) primarily uses canola oil, a resource-intensive agricultural product with implications for land use and food systems. Kaneka (Japan) and CJ CheilJedang/CJBio (Korea/Indonesia) similarly rely on plant oils such as rapeseed and palm, or sugar-rich feedstocks like cane, tapioca, and corn, inputs that embed substantial carbon and resource footprints.

A few companies have begun using waste resources to reduce costs. Bio-on (Italy) uses sugar-beet molasses and agricultural waste. Newlight Technologies (US) uses methane/biogas-based fermentation paired with air-derived CO_2. A sustainable proposition is the utilization of lignocellulosic biomass due to its abundant availability, which allows the coprocessing of a

wide range of cereal wastes for PHA biosynthesis.[24–26] However, the process has not been commercially developed. All literature resources on agricultural waste utilization for PHA biosynthesis primarily focus on laboratory-scale studies.[27,28] Process dynamics and life cycle environmental, economic and socioeconomic analyses are needed for scalable, sustainable, climate-resilient, and circular solutions.[29] The study by Lopez-Arenas (2017) showed that a fed-batch fermentation strategy for sucrose-based PHA production with *Azohydromonas australica* achieves high yield and productivity while enabling a competitively low-cost, low-impact process, delivering 0.36 w/w sucrose, a production cost of 2.6 US$ per kg, and a global warming potential (GWP) of 1.7 kg CO_2e per kg.[30] Sustainable techno-economic-environmental performance can only be determined by a dedicated waste-to-PHA dynamic simulation (DS), life cycle assessment (LCA), and techno-economic analysis (TEA) study. However, there is no DS-LCA-TEA study on PHA biosynthesis from lignocellulose, which is essential for its sustainability evaluation in industrial-scale waste-integrated biorefining. In addition, studies have shown no GWP reduction[18,19,23,31–33] or a significant increase in PHA production costs, which are twice or even seven times as much as those of fossil-based plastics.[34,35] Thus, both environmental and economic benefits need to be justified through a comprehensive LCA and TEA. DS, LCA, and TEA are interdependent, which has not been studied for PHA biocomposite biosynthesis from lignocellulose biomass. This study makes the following novel contributions: lignocellulosic biomass utilization for PHA biocomposite biosynthesis, and DS, LCA and TEA for scalability and sustainability, as follows. Moreover, it presents the best available industrial settings for lignocellulosic PHA to become sustainable.

Materials and methods

The methodology in Fig. 1 consists of a DS model verification, LCA and TEA. The DS model, discussed later, is solved as an optimization problem comprising differential equations corresponding to the mass balance of the main inlet and outlet components, applying the reaction kinetics, across the bioreactor, substrate, and nitrogen as inlet components, bacterial cell biomass within the bioreactor medium, and PHA as the outlet component, to minimize the error between experimental data and model predicted data on temporal PHA and cell biomass concentration profiles. Once the DS model-predicted profiles match the experimental profiles, the final bioreactor system parameters are noted. The final concentrations after PHA purification are used to determine the mass and energy balance at an industrial scale. The LCA and TEA performances of the whole PHA production flowsheet system are then evaluated. Before moving on to DS, LCA and TEA, metabolic pathways are discussed to show the responsible pathways for cellular PHA production.

Fig. 2 shows the contributing and competing metabolic pathways to PHA synthesis. From lignocelluloses, sugars (glucose and fructose) are extracted *via* cellulose and hemicellulose. Sugars are the substrates to feed the bacteria (*C. necator*), which, through the glycolysis pathway (yellow in Fig. 2), synthesize pyruvate. Glycerol, a byproduct of biodiesel production, is another alternative substrate, which, *via* the glycerol pathway (orange in Fig. 2), also leads to pyruvate (not studied in this paper). Pyruvate synthesizes acetyl-CoA (purple in Fig. 2). PHBs or the molecules of PHAs are synthesized *via* the PhaCAB pathway under nutrient-starving conditions (C : N > 80 : 20 w/w) (pink in Fig. 2).[12] In this pathway, two molecules of acetyl-CoA are condensed into acetoacetyl-CoA by the enzyme acetyl-CoA acetyltransferase (encoded by the gene *phaA*). Acetoacetyl-CoA is then reduced to produce 3-hydroxybutyryl-CoA, a reaction catalyzed by the enzyme Acetyl-CoA reductase (encoded by the gene *phaB*). In the final step, PHB is produced from 3-hydroxybutyryl-CoA *via* polymerisation by the enzyme Polyhydroxyalkanoate synthase (encoded by the gene *phaC*). An alternative to the PhaCAB pathway is the tricarboxylic acid (TCA) cycle (blue in Fig. 2) under normal nutrient conditions, which produces necessary energy for cell growth. Next, DS is developed for the mass balance models based on the experimental observations on substrate, cell biomass and PHA concentrations, as shown in the following section.

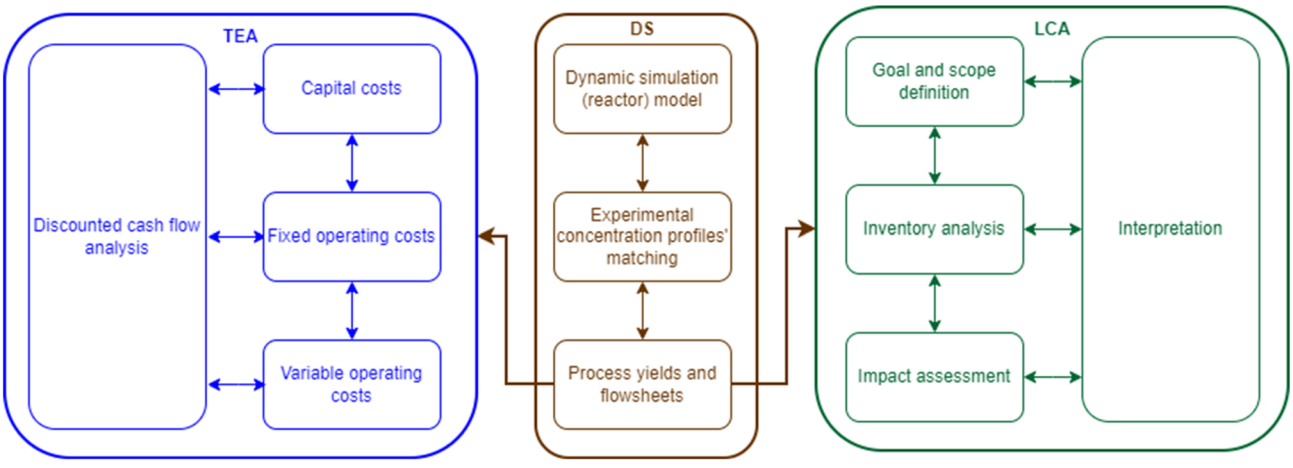

Fig. 1 Integrated DS, LCA and TEA framework.

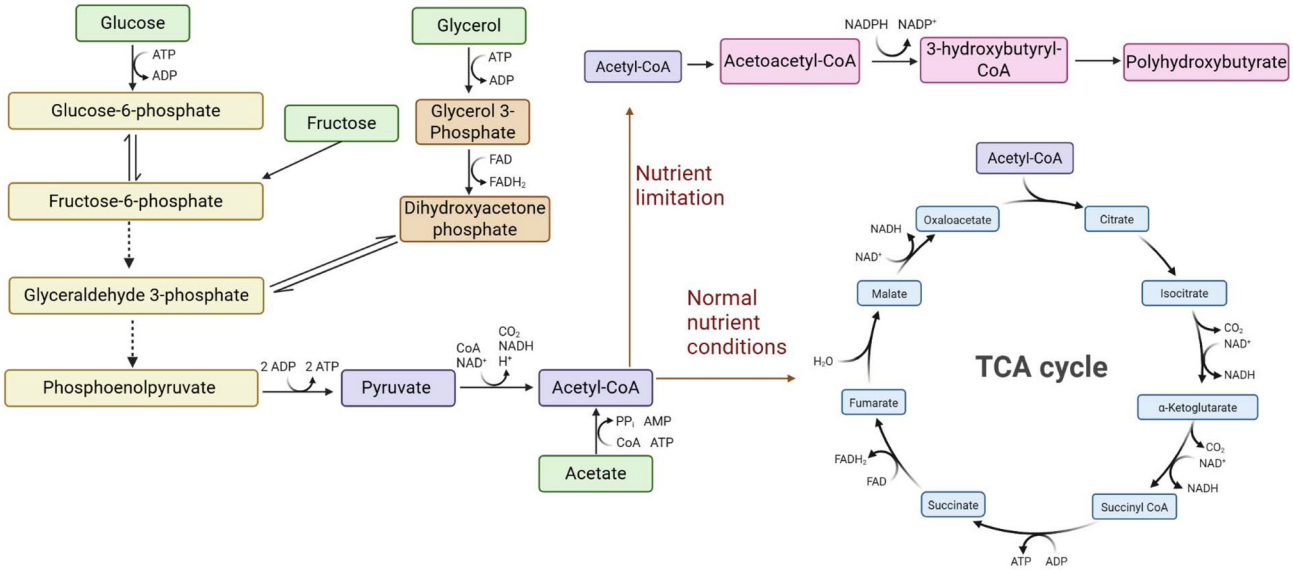

Fig. 2 Associated metabolic pathways of PHB biosynthesis in *C. necator*, highlighting the glycolysis pathway (yellow), glycerol pathway (orange), acetyl-CoA synthesis (purple), PhaCAB pathway for PHB/PHA synthesis (pink), and competing tricarboxylic acid (TCA) cycle (blue).

Dynamic simulation (DS) modeling

To better understand and optimize the fermentation process, a DS model is developed to describe the relationships among microbial cell biomass growth, substrate concentration, nitrogen concentration, and PHA (also includes polyhydroxybutyrate, PHB) production. A kinetic-based mass transfer model was formulated based on a set of reasonable assumptions. A parameter sensitivity analysis was conducted to evaluate their influence on the model performance. The model parameters were then calibrated using experimental data.

Assumptions. (1) Active microbial cell biomass concentration (C_X) and PHA concentration (C_P) are considered as state variables. (2) The oxygen and carbon dioxide concentrations are not treated as state variables, as the oxygen level is assumed to remain within a non-limiting and non-inhibitory range, and carbon dioxide is assumed to have no significant effect on the fermentation process. (3) The effect of cell death is neglected in the model. (4) Nitrogen concentration (C_N) and carbon substrate concentration (C_S) are treated as limiting nutrients. Nitrogen is assumed to contribute solely to microbial growth, whereas the carbon substrate is utilized for microbial growth, maintenance, and PHA accumulation.

Microbial cell biomass growth (C_X) is assumed to occur not only on the substrate (C_S) and ammonium (C_N), but also on the produced PHA (C_P). The reaction rates for microbial growth on substrate and ammonium, and on PHA, are given in eqn (1) and (2), respectively.[11]

$$\mu_{xs} = \mu_{xs}^{max}\left(\frac{C_S}{K_S + C_S + C_S^2/K_{IS}}\right)\left(\frac{C_N}{K_N + C_N + C_N^2/K_{IN}}\right) \times \left[1 - \left(\frac{C_X}{C_X^{max}}\right)^{\alpha}\right] \quad (1)$$

$$\mu_{xp} = \mu_{xp}^{max}\left(\frac{f_P}{K_P + f_P}\right)\left(\frac{C_N}{K_N + C_N + C_N^2/K_{IN}}\right)\left[1 - \left(\frac{C_X}{C_X^{max}}\right)^{\alpha}\right] \quad (2)$$

where K_S, K_N, and K_P are the saturation constants of substrate, nitrogen, and PHA for cell biomass growth, respectively; K_{IS} and K_{IN} are the inhibition constants for substrate and nitrogen for cell biomass growth, respectively; $f_P = P/X$ represents the ratio of PHA (C_P) to active cells (C_X); μ_{xs}^{max} and μ_{xp}^{max} denote the maximum specific cell biomass growth rate on substrate and PHA, respectively; C_X^{max} is the maximum active cell biomass concentration, and α is the cell density inhibition coefficient. The cell biomass growth on substrate is limited by excessively high or too low substrate concentration (C_S) and nitrogen concentration (C_N), as well as by very large cell density (C_X), as shown in eqn (1). Similarly, the cell biomass growth on PHA is constrained to the intracellular PHA fraction (f_P), nitrogen concentration (C_N) and cell density (C_X), as shown in eqn (2).

The PHA accumulation rate is limited by the nitrogen concentration (C_N), substrate concentration (C_S) and excessively high intracellular PHA fraction (f_P), which is modelled in eqn (3).

$$\mu_{ps} = \mu_{ps}^{max}\left(\frac{K_{PIN}}{C_N + K_{PIN}}\right)\left(\frac{C_S}{K_{PS} + C_S + C_S^2/K_{PIS}}\right)\left[1 - \left(\frac{f_P}{f_P^{max}}\right)^{\beta}\right] \quad (3)$$

where μ_{ps}^{max} denotes the maximum specific production rate; K_{PIN} and K_{PIS} represent nitrogen and substrate inhibition constants for PHA production, respectively; K_{PS} is the saturation constant for PHA production; f_P^{max} indicates the maximum PHA-to-cell biomass ratio, and β is the saturation exponent for PHA synthesis.

The mass balance is used to describe the relationship between the consumption of substrate and nitrogen and the growth and accumulation of cells and PHA. A fed-batch process is considered, in which the substrate and nitrogen are fed into the bioreactor to maintain their concentrations at desired levels. Let $F_S(t)$ and $F_N(t)$ denote the feed flowrates of the substrate and nitrogen, respectively. The concentrations of substrate and nitrogen can then be expressed as in eqn (4) and (5).

$$\frac{dC_S}{dt} = \frac{F_s(t)C_{S_F}}{V} - D(t)C_S - \left(\frac{\mu_{xs}}{Y_{xs}} + \frac{\mu_{ps}}{Y_{ps}} + m_s\right)C_X(t) \quad (4)$$

$$\frac{dC_N}{dt} = \frac{F_N(t)C_{N_F}}{V} - D(t)C_N - \left(\frac{\mu_{xs} + \mu_{xp}}{Y_{xN}}\right)C_X(t) \quad (5)$$

where Y_{xs}, Y_{ps}, and Y_{xN} indicate the cell and PHA yields on the substrate, and the cell yield on nitrogen, respectively; m_s is the substrate consumption rate for maintenance; C_{S_F} and C_{N_F}, are the substrate and nitrogen concentrations in the given feed method, respectively; the dilution rate, $D(t) = F(t)/V(t)$, is defined as the ratio of the overall flowrate $F(t)$ to the biorctor volume $V(t)$. The substrate consumption arises from two main sources: feeding, represented by the first two terms in eqn (4), and biological utilization, which includes cell biomass growth, PHA synthesis, and cell maintenance, represented by the third term. Similarly, the nitrogen consumption results from feeding (the first two terms in eqn (5)) and cell biomass growth and PHA-associated metabolism, described by the last term of that equation. The overall flowrate, $F(t)$ in eqn (4) and (5), comprises the substrate feed flowrate $F_S(t)$ and nitrogen feed flowrate $F_N(t)$, and is expressed as in eqn (6).

$$F(t) = \frac{dV(t)}{dt} = F_s(t)\frac{\rho_{FS} - C_{S_F}}{\rho_w} + F_N(t)\frac{\rho_{FN} - C_{N_F}}{\rho_w} \quad (6)$$

where ρ_{FS} and ρ_{FN} represent the density of substrate and nitrogen in the given feed solution, respectively.The biomass concentration accounts for cell growth on both the external substrate and the intracellular PHA, as well as the dilution effect resulting from feed addition. The PHA concentration reflects its formation from the substrate, the consumption associated with cell biomass growth, and the dilution caused by the increasing reactor volume during feeding. Thus, the cell biomass and PHA concentrations are shown in eqn (7) and (8).

$$\frac{dC_X}{dt} = (\mu_{xs} + \mu_{xp} - D(t))C_X(t) \quad (7)$$

$$\frac{dC_P}{dt} = \left(\mu_{ps} - \frac{\mu_{xp}}{Y_{xp}}\right)C_X(t) - D(t)C_P(t) \quad (8)$$

wherein, Y_{xp} denotes the cell biomass yield on the PHA. Since the fed-batch operation maintains constant substrate and nitrogen concentrations, the dilution rate $D(t)$, in eqn (7) and (8), can be determined by setting eqn (4) and (5) to zero and combining them with eqn (6). This special case is analyzed in the results and discussion.

Model calibration and validation. The model developed above is calibrated and validated using experimental data obtained from a study that employed cereal waste as the feedstock and *C. necator* as the microorganism.[27] Before calibration, a relative sensitivity analysis of the model was conducted to guide the parameter adjustment. The relative sensitivity function[11] is defined as in eqn (9) and (10).

$$\delta = \frac{\sum_{i=1}^{t}\left(\frac{\partial y_i(t)}{\partial\theta}\frac{\theta}{y_i(t)}\right)}{n} \quad (9)$$

$$\frac{\partial y_i(t)}{\partial\theta} = \lim_{\Delta\theta\to 0}\frac{y_i(t,\theta+\Delta\theta) - y_i(t,\theta)}{\Delta\theta} \quad (10)$$

where in $y_i(t)$ denotes the variable of interest; n indicates the total number of selected data points, and θ represents the model parameter under analysis; the small perturbation of θ, denoted as $\Delta\theta$ is defined as $\Delta\theta = p\theta$ where $p = 10^{-4}$. In this study, the cell biomass (C_X) and PHA concentration (C_P) are considered as target variables.

The model was calibrated by minimizing the sum of squared errors (SSE) between the estimated and experimental values, while the Nash–Sutcliffe model efficiency coefficient[36] was employed to evaluate model performance. The corresponding equations for the sum of squared errors (eqn (11)) and the efficiency coefficient (eqn (12)) are as follows.

$$j(\theta) = \sum_{i=1}^{t}\left(y_i(t) - y_i{}^m(t,\theta)\right)^2 \quad (11)$$

$$E = 1 - \frac{\sum_{t=0}^{T}(y_t - y_t{}^m)^2}{\sum_{t=0}^{T}(y_t - \bar{y})^2} \quad (12)$$

where $y_i(t)$ and $y_i{}^m(t, \theta)$ represent the experimental data and model estimated values of the corresponding variables, respectively, which are the cell biomass (C_X) and PHA concentration (C_P) in this paper; $\bar{y}$ denotes the mean value of experimental data.

Life cycle assessment (LCA)

LCA is a standardized methodology for assessing the environmental impacts of cradle-to-grave (from raw material extraction to end-of-life resource circularization) systems. According to the ISO14040-44, LCA comprises four interactive stages: goal and scope definition, inventory analysis, impact assessment and interpretation.[37]

Goal and scope definition. The functional units and system boundaries are defined in the goal and scope definition. In addition, inventory databases and impact assessment methods are selected through interactive stages. In this case, the functional unit is 1 ktpa (kilotons per annum) of PHA-biocomposite manufacturing for inventory data collection. This functional unit has been decided based on the economic feasibility of the manufacturing system, as discussed in the section on TEA. The techno-economic feasibility of the system increases with increasing PHA biocomposite throughput. A 1 ktpa PHA-biocomposite manufacturing provides an acceptable net cash

flow, illustrated later in the section on TEA. The life cycle impact assessment results have been presented per kg PHA biocomposite basis for comparison against the literature as well as fossil-based equivalent polypropylene systems. Both the cradle-to-gate and cradle-to-grave GWP results have been shown. The substitution method has been applied, which allows the total environmental impact calculation in each impact category of the system, compares the system with other equivalent systems and calculates the environmental impact savings from substituting fossil-based equivalent systems. The allocation method is not appropriate in this case because the electricity generation would have negligible environmental impact savings compared to fossil-based incumbents. According to the guidelines by the ISO14040 series and ISO4060 series, LCA reporting must be conservative, which has been adopted in this case. This means that the GWP savings from on-site excess electricity generated to displace the grid electricity are separately reported.

Process description. Fig. 3 shows the integrated PHA copolymer synthesis, PHA-biocomposites' 3D manufacturing and end-of-life recycling with fresh materials. The PHA-biocomposite manufactured includes recyclate, for which the current plastics recycling rate has been assumed.

The average concentration of lignocellulosic biomass and its subsequent flows to various process units or into products, scaled to the functional unit from laboratory experiments, are shown later in Results and Discussion. Lignocellulose biomass can be wide-ranging, including a mix of various feedstocks, such as agricultural wastes or corn and maize stover, wheat and rice straw, sugarcane bagasse and molasses, sugar beet molasses, *etc*. The process begins with handling waste (in this case, lignocellulosic) biomass to generate dry biomass. This is followed by biomass fractionation into soluble sugars (C5 and C6 monosaccharides), cellulose fibers, and insoluble lignin. The biomass handling and fractionation phase follows the previous studies,[38,39] detailed in the SI. The main processes involved in converting biomass into PHAs are biomass handling and fractionation, fermentation, and PHA recovery (Fig. 3).

Extracted sugars from the pretreatment stage, discussed in the SI, are directed to the fermenter, while the cellulose fibers are extruded for PHA biocomposite synthesis, and insoluble lignin is used for combined heat and power (CHP) generation. The flashed vapour from the slurry reactor is condensed and sent to the wastewater treatment plant (WWTP), attached to an anaerobic digestion (AD), followed by CHP generation from the biogas.

The nutrient medium for microorganisms comprises three solutions added to a mix of vitamins (DSMZ, 2011),[40] detailed in the SI. Fig. S1 shows the sequential reactors with cultivation (nutrient-enriched or feast) and copolymer accumulation (starvation or famine) in two reactors, respectively. Over 75% cdw PHA copolymers' accumulation is obtained with *C. necator*, *e.g.*, >90% with H16 strain,[12] 80% with B-10646 strain,[28] and over 75% with DSM 545.[27] PHA copolymer yield is obtained from the DS simulation modelling results matched with the experimental profiles, shown later. PHA copolymers are then recovered and purified *via* filtration, centrifugation, solvent extraction using the natural deep eutectic solvent (NDES), washing and drying. The recovered spent cell biomass can be recirculated to supplement the microbial culture.[26] The NDES is recovered to minimize the make-up NDES input into the system. The purified PHA copolymer matrix is reinforced with extracted cellulose fibers from the biomass fractionator to form fresh PHA biocomposites. A range of PHA biocomposite properties must meet the property standards; Table S1 shows the properties, standards, analytical equipment used to test these properties, PHA properties before and after reinforcement, and a comparison with fossil-based polypropylene. Fig. S2 shows the engineering stress-strain tensile test and FTIR results. These results confirm the copolymers and biocomposites' desired qualities, aligning closely with the fossil-based equivalent plastic properties. The PHA composites can meet the same properties as the fossil-derived polypropylene after reinforcing PHA copolymers with (0.1–0.2 w/w) cellulose fiber biofillers. The fresh PHA biocomposites may be admixed with PHA biocomposite recyclate for 3D manufacturing of PHA

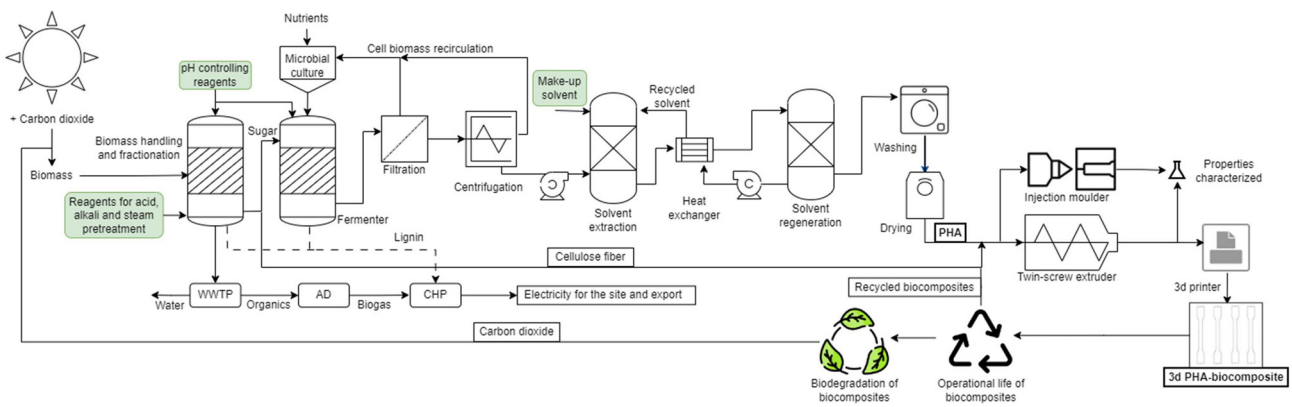

Fig. 3 PHA biocomposite integrated manufacturing: cradle-to-cradle system configuration. The external reagent inputs needed are highlighted for LCI data collection.

biocomposites, following extrusion and 3D printing. A 47% recycling rate is assumed, the same as for plastic pots, tubs, and trays,[41] which are among the end uses of PHA biocomposites. The balance of PHA biocomposites not recycled would biodegrade in any environment, including marine, soil, freshwater, and aerobic environments, releasing embedded carbon as carbon dioxide. Carbon dioxide is sequestered during photosynthesis, closing the loop of biomass valorization.

Life cycle inventory analysis. To establish the life cycle inventory databases for input resources, all available LCA studies on PHA synthesis in the literature have been consulted. There are only 6 studies on the LCA of PHA production systems,[18,19,23,31–33] among which, the first 4 studies[18,19,23,31] can be reproduced and validated as they made the inventory data transparently or accurately available. This validation, shown later, demonstrates appropriate life cycle inventory database selections. The foreground system's (Fig. 3) input inventory flows and their corresponding background life cycle inventory databases selected, as well as background life cycle inventory databases selected for the equivalent output products to be displaced, corresponding to the functional unit of 1 ktpa PHA biocomposite manufacturing, are shown in Table 1. Fig. 3 highlights the input reagents to the PHA biocomposite manufacturing system. Global databases were preferred over EU (RER) or RoW (rest of the world) to represent their global supply chains. In case of their absence, the other geographic regions were chosen chronologically for the selected databases. Cut-off databases were selected for this study. In the absence of Cut-off data, 'At the Point of Substitution' (APOS) data has been used.[42] Sodium hydroxide, the most common resource input to control the fermenter's pH at 6.8, varies between 0.136 and 0.4 w/w of the product.[19,23] Citric acid and lime are also used to control pH when it rises above 6.8.[19] Sodium hypochlorite and chloroform, the most common solvents used, provide 85% and 99% recovery and purity of PHA, and vary 0.13–0.34 and 0.06–0.73 w/w of product, respectively.[19,23,31] In addition, surfactants and dimethyl carbonate are other solvents reported (0.53 and 0.19 w/w of product, respectively) to extract PHA copolymers.[31,32] In this case, however, NDES replaces chemical solvents that are more environmentally detrimental. In the absence of a life cycle inventory database for the NDES, "Maize starch {RoW}| production | Conseq" has been selected to represent a natural form of DES. Similarly, a representative chemical life cycle inventory database has been chosen, where the exact nutrients for the incubation and culture growth stages were unavailable. Considering the density difference between PHA biocomposites and polypropylene to be displaced (Table S1), the polypropylene amount range is shown in Table 1. Although for a conservative estimation of GWP saving from the displacement, an equal amount of displacement is considered. Such an assumption is in accordance with the ISO14040 series (LCA) and ISO14060 series (carbon footprint calculations). Large-scale plants require far less electricity, 4.78–23.04 MJ kg^{-1} product,[19,31,32] and heat, 0.72–2.2 MJ kg^{-1} product,[19,31] respectively, compared to pilot[23] or laboratory-scale systems (>100 MJ kg^{-1} product) due to the overall process heat integration. Furthermore, the feasibility of biorefineries lies in the self-generation of electricity through onsite CHP from the remaining unconverted biomass, *i.e.*, recovered lignin and

Table 1 Foreground inventory flows for 1 ktpa PHA biocomposite manufacturing and their selected life cycle inventory (LCI) database names

Database name	Inventory (purpose) (input)	Quantity	Unit
Ecoinvent 3.10: sodium hydroxide, without water, in 50% solution state {GLO}| market for | cut-off	Sodium hydroxide (pH control)	0.40	ktpa
Ecoinvent 3.10: sulfuric acid {GLO}| market for | cut-off	Sulfuric acid (biomass pretreatment)	0.20	ktpa
Maize starch {RoW}| production | conseq.	NDES (solvent)	0.10	ktpa
Ecoinvent 3.10: citric acid {GLO}| market for | cut-off	Citric acid (pH control)	0.0025	ktpa
Ecoinvent 3.10: lime, hydraulic {RER}| market for lime, hydraulic | cut-off	Lime (pH control)	0.01	ktpa
Monoammonium phosphate {RER}| market for monoammonium phosphate | cut-off	Potassium dihydrogen phosphate (nutrient)	0.115	ktpa
Sodium phosphate {RER}| market for sodium phosphate | cut-off	di-sodium hydrogen phosphate dihydrate (nutrient)	0.145	ktpa
Ammonium chloride {GLO}| market for | cut-off	Ammonium chloride (nutrient)	0.050	ktpa
Magnesium sulfate {GLO}| market for | cut-off	Magnesium sulfate (nutrient)	0.025	ktpa
Calcium chloride {GLO}| market for | cut-off	Calcium chloride (nutrient)	0.0005	ktpa
Manganese {GLO}| market for | cut-off	Manganese(II) chloride tetrahydrate (nutrient)	0.00025	ktpa
Chemical, organic {GLO}| market for | cut-off	All other nutrients, including vitamins in traces	0.00053	ktpa
Ecoinvent 3.10: water, deionised {RoW}| market for water, deionised | cut-off	Water (pretreatment, washing)	0.11	ktpa
ELCD: process steam from natural gas, heat plant, consumption mix, at plant, GB System	Heat (biomass fractionation and solvent recovery unit)	2.20	TJ
Transport, freight, lorry 3.5–7.5 metric ton, €5 {RoW}| market for transport, freight, lorry 3.5–7.5 metric ton, €5 | cut-off	Transport	100	ktkm
Wastewater, average {RoW}| treatment of, capacity 1E9l per year | cut-off	WWTP	3876.00	m^3
	Inventory (products that can be displaced)		
Polypropylene, granulate {RER}| production | cut-off	Polypropylene	1–1.4	ktpa
Electricity, high voltage {RER}| market group for | cut-off	Electricity	1.26	GWh

biogas from WWTP and AD.[37–39] All electricity needs must be met by onsite CHP generation for the economic feasibility of any biorefinery systems.[26,37] Typically, 70% of the biorefinery site electricity requirements can be fulfilled by onsite CHP generation,[19,37–39] utilizing the remaining unconverted biomass, mainly recovered lignin, and biogas from WWTP and AD. At 20 MJ kg^{-1} of the overall low heating value of recovered biogas and lignin and 35% electricity generation efficiency,[43–46] the amount of electricity generated by the integrated PHA biocomposite manufacturing system (Fig. 3) is 4 GWh at 290 operating days per year for 1 ktpa PHA biocomposite production capacity. The electricity consumption by the PHA biocomposite manufacturing system (Fig. 3) is 2.6 MWh t^{-1} biocomposite. After meeting this electricity demand by the site, the net available excess electricity is 1.26 GWh. This electricity can be injected into the grid and can give further savings in the environmental impacts from displacing the grid electricity. However, the credit from electricity generation has been separately reported for a conservative approach following the ISO14040 series and ISO14060 series guidelines. The electricity consumption by the PHA copolymer biosynthesis (2.6 MWh t^{-1}) in this study[38,39] is similar to that in the published literature,[19] which also showed excess electricity generation and export utilizing the fermenter outlet and wastewater-derived biogas.

Life cycle impact assessment (LCIA). The LCIA method selected is ReCiPe 2016 (M: midpoint) (H: Hierarchist), as it has a global consensus.[47] The main impact category analyzed is GWP100 years, using characterisation factors last updated in the IPCC 6th Assessment Report (AR6). LCIA results are detailed later in the Results and discussion.

Interpretation. The interpretation includes the validation of GWP against the literature, all ReCiPe 2016 (M) (H) characterization factors' reporting and multivariable uncertainty analysis using Monte Carlo simulation.[50] The inventories' base values, as shown in Table 1, vary as discussed in the life cycle inventory analysis, to capture their effects on the life cycle impact categories. The LCA interpretation stage is discussed in detail later in the Results and discussion.

Techno-economic analysis (TEA)

TEA comprises the analyses of capital and operating costs, product value and net present value, according to the standard engineering correlations.[26,37] This section shows the standard TEA methodology and equations.[51] The capital cost is annualized and added to the operating cost. The traded product value is calculated on an annual basis. The difference between the product value and the total cost, both on an annual basis, gives the economic margin of the system. The payback time is estimated from the discounted cash flow or net present value analysis plot.

The capital cost is estimated using eqn (13). To arrive at this equation, first, a suitable base delivered cost (DC_i) and the size (base $size_i$), to which the delivered cost applies, of a unit (i) is found in the literature or obtained from the vendor. This delivered cost is updated to the current given size (present $size_i$) by applying a scale factor (R_i). The scale factor is around 0.6 and indicates that for a dimensionless size ratio (present $size_i$/base $size_i$) > 1, the updated delivered cost will be less than the linear proportional increase, presenting an economy of scale. The delivered cost of individual equipment is further updated by applying a ratio of the chemical engineering plant cost index between the present year ($CEPCI_{i,\ present\ year}$) and the year corresponding to DC_i ($CEPCI_{i,\ base\ year}$). The aggregation of delivered costs of all units is applied to a Lang factor (lang factor) to obtain the total capital cost (capital cost). Within the Lang factor, an installation factor of 0.39 to the delivered cost of equipment is included.[26]

$$\text{Capital cost} = \left(\sum_i DC_i \times \left(\frac{\text{present size}_i}{\text{base size}_i}\right)^{R_i} \times \left(\frac{CEPCI_{i,\text{present year}}}{CEPCI_{i,\text{base year}}}\right)\right) \times \text{lang factor} \quad (13)$$

Capital cost is the total capital cost of the entire system. DC_i is the delivered cost of a unit i. The base $size_i$ is the size of the unit i for which the delivered cost (DC_i) applies. The present $size_i$ is the current given size of the unit i. R_i is the scale factor to update the delivered cost of the unit i. $CEPCI_{i,\ present\ year}$ is the chemical engineering plant cost index of the present year. $CEPCI_{i,\ base\ year}$ is the chemical engineering plant cost index of the base year corresponding to the base delivered cost of equipment corresponding to DC_i. Lang factor is 3, meaning that the total capital cost is three times the total delivered cost of equipment.[38,39] Next, the annual capital cost is calculated using eqn (14). The annual capital cost (Capex) is the product of an annual capital charge (annual capital charge) and the total capital cost (capital cost).

$$\text{Capex} = \text{annual capital charge} \times \text{capital cost} \quad (14)$$

Capex is the annual capital cost.

Annual capital charge is the charge applied annually on the total capital cost.

The operating cost is the summation of the fixed, variable, feedstock and miscellaneous costs. The fixed operating cost comprises two components. One part is dependent on indirect capital cost, and the other on labor cost. The indirect capital cost-dependent fixed operating cost items are maintenance (5–10% of the indirect capital cost), capital charges (10% of the indirect capital cost), insurance (1% of the indirect capital cost), local taxes (2% of the indirect capital cost) and royalties (1% of the indirect capital cost), *i.e.*, a total of 0.24 times the indirect capital cost, which is 25% of the annual capital cost for solid–fluid processing systems. Thus, for the solid–fluid system, the indirect capital cost-dependent fixed operating cost is 0.06 times or (0.24 × 0.25) the annual capital cost, as shown in eqn (15).

$$\text{Indirect capital cost dependent fixed operating cost} = 0.06 \times \text{Capex} \quad (15)$$

The labor cost-dependent fixed operating cost items are personnel, laboratory, supervision and plant overheads, 100%,

20%, 20% and 50% of the labor or personnel cost. Thus, the labor cost-dependent fixed operating cost is 1.9 times the labor cost, as shown in eqn (16).

$$\text{Labor cost dependent fixed operating cost} = 1.9 \times \text{labor cost} \quad (16)$$

The fixed operating cost is the summation of the indirect capital cost-dependent fixed operating cost and the labor cost-dependent fixed operating cost, as shown in eqn (17).

$$\text{Fixed operating cost} = \text{indirect capital cost dependent fixed operating cost} + \text{labor cost dependent fixed operating cost} \quad (17)$$

The variable cost includes the cost of utilities and reagents, as shown in eqn (18).

$$\text{Variable cost} = \text{cost of utilities and reagents} \quad (18)$$

The feedstock cost is another component of the operating cost. The miscellaneous operating cost includes sales expense, general overheads, and research and development, totaling 20–30% of the aggregated fixed operating cost and variable cost, as shown in eqn (19).

$$\text{Miscellaneous operating cost} = 0.3 \times (\text{fixed operating cost} + \text{variable cost}) \quad (19)$$

The operating cost (Opex) is the summation of the fixed operating cost, variable cost, feedstock cost and miscellaneous operating cost, as shown in eqn (20).

$$\text{Opex} = \text{fixed operating cost} + \text{variable cost} + \text{feedstock cost} + \text{miscellaneous operating cost} \quad (20)$$

The product value is the summation of the multiplications between unit price and flowrate of a product, as shown in eqn (21).

$$\text{Product value} = \sum_j \text{unit price}_j \times \text{flowrate}_j \quad j \in \text{product} \quad (21)$$

Product value is the total value of all products from the system. Unit price$_j$ is the price of a unit flowrate of a product j. Flowrate$_j$ is the flowrate of the product j. j is the product index. Product is the product set.

The net present value (NPV$_y$) in a given year y is calculated using eqn (22).

$$\text{NPV}_y = \text{NPV}_{y-1} + \frac{(\text{product value} - \text{Opex} - \text{Capex})}{(1 + \text{IRR})^y} \quad (22)$$

NPV$_{y=0}$ = capital cost, IRR is the internal rate of return (in fractional value). Eqn (13)–(22) are sequentially applied with input parameters, delivered cost, base size, current size, annual capital charge, labor cost, unit prices and flowrates of products, utility and reagent costs (unit cost times consumption rate of each), feedstock costs (unit cost times flowrate) and internal rate of return, to ultimately obtain the discounted cash flow profile of the system. Apart from the flowrates, which are specific to the process system, all other input parameters are market-dependent macro-economic parameters. Any uncertainty can be analyzed through sensitivity analysis of input parameters on the discounted cash flow profile or any other output variables in eqn (13)–(22). The sizes or flows of each unit involved in Fig. 3 are shown in Table 2, which shows the calculation of the delivered cost of equipment (DC$_i$) and the total capital cost (capital cost) (eqn (1)) corresponding to 1 ktpa of PHA manufacturing. The cost and size parameters or bases to calculate them are shown in Sadhukhan *et al.* (2014).[26]

The market data for the operating cost and net present value analyses in Table 3 include the prices of average chemical reagents (sodium hydroxide, sulfuric acid, NDES, citric acid, lime, and water, as listed in Table 1), electricity and heat, lignocellulosic biomass, and PHA biocomposites. The PHA biocomposite price varies, US$7–20 per kg,[35] US$4–15,[48] and US$4–9 per kg.[49] A base price of US$7 per kg is thus considered to establish the economic viability of the PHA biocom-

Table 2 Sizes, delivered cost of equipment, and total capital cost for 1 ktpa of PHA manufacturing

Unit	Base cost, million US$	Scale factor	Base size	Unit	CEPCI-base year	Current size	Current costs, million US$
Inoculation	0.26	0.6	3.53	tph	402	0.44	0.15
Fermenters	0.67	0.8	1.04	tph	402	0.44	0.69
Centrifugation	2.92	0.7	18.466	tph	402	0.44	0.44
Solvent extraction-recovery	2.96	0.7	18.466	tph	402	0.44	0.44
Washing	0.41	1	33.5	tph	394.3	0.44	0.01
Drying	7.6	0.8	33.5	tph	394.3	0.44	0.50
Anaerobic digestion	1.54	0.6	43	tph wastewater	402	1.89	0.48
CHP	1		5	GWh		3.99	0.80
Biomass handling	14.1	0.78	83.3	tph biomass	402	2.10	1.63
Biomass fractionation	5.62	0.78	83.3	tph biomass	402	0.50	0.21
Twin-screw extrusion	0.08	1	1	tph	820	0.15	0.01
Injection moulding	0.10	1	1	tph	820	0.15	0.02
3D printing	0.08	1	1	tph	820	0.15	0.01
Delivered cost of equipment							5.39
Total capital investment							16

Table 3 The quantities and costs for operating cost and net present value analyses

	Quantity	Unit	Price	Unit	Reference for unit price
Reagents	1.2	ktpa	0.26	US$ per kg	Business Analytiq (2025)[52]
Electricity	−4.5	TJ	0.06	US$ per MJ	Ofgem (2025)[53]
Heat	2.2	TJ	0.29	US$ per MJ	Ofgem (2025)[53]
Annual capital charge	0.1				Sadhukhan *et al.* (2025)[42]
Internal rate of return	0.1				Sadhukhan *et al.* (2025)[42]
Lignocellulose biomass	3.5	ktpa	100	US$ per dry t	Langholtz *et al.* (2022)[54]
PHA biocomposite	1	ktpa	7–20	US$ per kg	Levett *et al.* (2026)[49]

posite production system (Fig. 3). Table 3 also shows the annual capital charge and internal rate of return.

Results and discussion

DS modeling

The experimental data on PHA and cell biomass concentration dynamics presented in Bellini *et al.* (2024) were extracted using the online tool WebPlotDigitizer. The initial substrate and nitrogen concentrations were 12 g L^{-1} and 0.64 g L^{-1}, respectively. The initial cell biomass concentration was 0.13 g L^{-1}, respectively. There was no PHA in the system to start with. Two ways the DS model equations (eqn (4)–(8), integrated with eqn (1)–(3)) were solved, variable and constant substrate and nitrogen concentrations, C_S and C_N, in the reaction medium. The open source GitHub codes (https://github.com/ritamsen74/pha_optimisation/blob/main/dynamicsim.py and https://github.com/nicolehu0306-crypto/Dynamical-modelling-of-PHA-production for variable and constant substrate and nitrogen concentrations in the reaction medium) of the model (eqn (4)–(8), integrated with eqn (1)–(3)) were implemented in Python 3.12 and solved using Runge-Kutta (4,5) or ode45 method and the Euler method for the ordinary differential equations (ODEs), respectively.

According to eqn (9) and (10), the relative sensitivity of the model based on the experimental data is summarized in Table 4. When $\delta > 0$, the variable $y_i(t)$ increases with increasing θ; conversely, $\delta < 0$ implies that the variable $y_i(t)$ decreases as θ. The parameters with $|\delta| > 0.5$ are deemed to be sensitive to the variables. From Table 4, it can be concluded that parameters K_{IN}, K_N, K_{PIN} μ_{xs}^{max}, and μ_{ps}^{max} are sensitive.

Besides the sensitivity results K_{IN}, K_N, K_{PIN} μ_{xs}^{max}, and μ_{ps}^{max}, the parameters μ_{xp}^{max} and C_{S_F} were also varied across experimental conditions. This adjustment is justified because μ_{xp}^{max} directly affects the rate of cell biomass growth on PHA, while C_{S_F} corresponds to the substrate concentration in the feed, which changes with the feeding strategy. The global optimization algorithm, differential evolution, implemented in Python, was employed to optimize the model parameters based on the minimization of the efficiency coefficient in eqn (12), to closely match the model-predicted PHA and cell biomass concentrations with experimental values, with equal weighting allocated to their individual efficiency coefficients. The calibrated parameter values are shown in Table 5. The remaining parameters are the same as those used in the referenced experiments and articles, as shown in Table 6. Using these parameters, the ODEs, eqn (4)–(8), integrated with eqn (1)–(3), were solved. Fig. 4 shows the temporal evolution of cell biomass and PHA concentrations, comparing model predictions with experimental data, for two instances, treating C_S and C_N as variables as shown in eqn (4) and (5) and assuming C_S and C_N as constants, *i.e.*, eqn (4) and (5) equating to zero. In both cases, after 30 hours, the PHA concentration reaches the maximum at 6.6 g L^{-1}. In the case of variable substrate and nitrogen concentrations, PHA concentration declines after the maximum due to cell biomass growth at the expense of PHA in the starving medium. This also reinstates the need for keeping substrate and nitrogen concentrations constant in the medium, as shown in the second instance in Fig. 4. The product PHA must be with-

Table 4 Relative sensitivity of model parameters for cell biomass and PHA concentration

Parameter	K_S	K_{IS}	K_{IN}	K_N	K_{PS}	K_{PIS}	K_P	K_{PIN}
C_X	−0.3633	0.4524	0.5521	−0.5135	−0.0103	0.0008	−0.0287	0.0167
C_P	−0.3856	0.4802	0.5688	−0.5291	−0.4427	0.0337	0.0395	0.7211

Parameter	C_X^{max}	f_p^{max}	α	β	m_s	Y_{PS}	Y_{XN}	Y_{XP}
C_X	0.2198	−0.0000	0.0153	−0.0000	−0.0013	0.0074	0.0002	0.0023
C_P	0.0601	0.0000	0.0115	0.0002	−0.0035	0.0195	0.0005	0.0753

Parameter	Y_{XS}	μ_{xs}^{max}	μ_{ps}^{max}	μ_{xp}^{max}	C_{S_F}	C_{N_F}
C_X	0.0199	2.3300	0.0236	0.0298	0.0607	0.0013
C_P	0.0416	2.4726	1.0163	−0.0412	0.1386	0.0028

Table 5 Modified parameters for the model fitting with experimental data

Parameter	Estimated value	Modified value	Unit	Reference
K_{IN}	1.5	9.38	g N per L	Lee *et al.* (1997)[55]
K_N	0.254	0.52	g N per L	Patnaik (2006)[56]
K_{PIN}	0.262	0.30	g N per L	Mozumder *et al.* (2014)[11]
μ_{xs}^{max}	0.41	0.31	g cell per g cell per h	Du *et al.* (2001)[57]
μ_{ps}^{max}	0.217	1.34	g cell per g cell per h	Mozumder *et al.* (2014)[11]
μ_{xp}^{max}	0.126	0.19	g PHA per g cell per h	Mozumder *et al.* (2014)[11]
C_{S_F}	650	63.34	g L^{-1}	Mozumder *et al.* (2014)[11]

Table 6 The remaining parameters for the model based on references

Parameter	Value	Unit	Reference
Stoichiometric parameters			
Y_{PS}	0.35	g PHA per g substrate	Mozumder *et al.* (2014)[11] (experimentally determined)
Y_{XN}	8.9	g cell per g N	Mozumder *et al.* (2014)[11] (theoretically calculated)
Y_{XP}	0.88	g cell per g PHA	Dias *et al.* (2005)[22]
Y_{XS}	0.52	g cell per g substrate	Tanadchangsaeng and Yu (2012)[58]
Kinetic parameters			
K_S	1.2	g substrate per L	Cougnon *et al.* (2011)[59]
K_{IS}	16.728	g substrate per L	Mozumder *et al.* (2014)[11]
K_{PS}	4.1	g substrate per L	Lee *et al.* (1997)[55]
K_{PIS}	80	g substrate per L	Mozumder *et al.* (2014)[11]
K_P	0.48	g PHA per L	Mozumder *et al.* (2014)[11]
C_X^{max}	68	g cell per L	Mozumder *et al.* (2014)[11] (experimentally determined)
m_s	0.02	g substrate per g cell per h	Frigon *et al.* (2006)[60]
J_P^{max}	3.3		Mozumder *et al.* (2014)[11] (experimentally determined)
α	5.8		Mulchandani and Luong (1989)[61]
β	3.85		Dias *et al.* (2005)[22]
Operating parameters			
C_{N_F}	164		Mozumder *et al.* (2014)[11]
ρ_{FS}	1230		Mozumder *et al.* (2014)[11]
ρ_{FN}	1040		Mozumder *et al.* (2014)[11]
ρ_W	1000		Mozumder *et al.* (2014)[11]

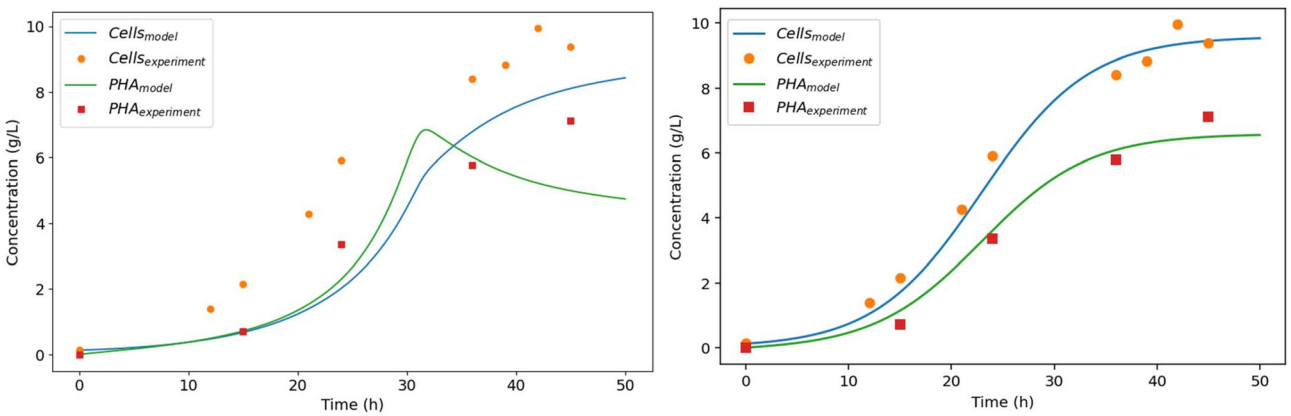

Fig. 4 The model and experimental data fitting of cell and PHA concentrations with time in two instances: variable substrate and nitrogen concentrations (left) and constant substrate and nitrogen concentrations (right).

drawn after it reaches the maximum concentration (in this case, after 30 h) in the fed-batch reactor to utilize the outlet stream with the highest PHA concentration in the downstream PHA separation and purification processes (Fig. 3 and Fig. S1). Based on eqn (12), the Nash-Sutcliffe model efficiency coefficients are E = 0.87 and 0.98 for PHA and E = 0.67 and 0.99 for cell biomass, in the two instances, further confirming the reliability and effectiveness of the dynamic model, especially for the second instance, when the substrate and nitrogen concentrations are kept constant in the fed-batch reactor.

The DS results in Tables 5, 6 and Fig. 4 of the bioreactor provide a representation of the process behaviour over time,

capturing variations in cell growth and product formation under realistic operating conditions. These time-resolved data, integrated with LCA and TEA, enable a consistent evaluation of environmental and economic performance with the resulting process dynamics in Fig. 4. The highest initial substrate concentration is 12 g L^{-1}. The maximum PHA product (copolymer) concentration is 6.6 g L^{-1} (Fig. 4). This gives a ratio of 0.55 between the maximum PHA production and initial substrate concentration, which forms the basis for the plant-wide mass balance, as shown in the following section.

LCA

The mass and energy balance, LCA and TEA models have been made available *via* open-source software with a user-friendly graphical interface: https://clovecircle.com/standalone/PHA-from-lignocellulose-lca-tea.html. The mass balance for the 1 ktpa PHA biocomposite manufacturing plant and how the flows interact are shown in Fig. 5. It starts with the average biomass (without ash and moisture) concentrations (24–36% hemicellulose, 38–54% cellulose, and 15–25% lignin, as shown in the methodology section). Biomass fractionation extracts 95% and 87% of hemicellulose and cellulose, respectively, as the sugar substrate for fermentation. PHA copolymer accumulation in the fermenter is 55% of the sugar substrate, as derived from the DS simulation results (Fig. 4). A further 65% recovery efficiency of PHA through the separation train to the biocomposite manufacturing section gives an overall PHA copolymer to sugar substrate ratio of 0.35.[11] Finally, the PHA copolymers and cellulose fibers are extruded or molded (at 95% efficiency) to design the PHA biocomposites with an 80 : 20 mass ratio to meet the properties in Table S1.

In order to validate the life cycle inventory database selections, as shown in Table 1, the literature-based LCA study results on PHA production have been reproduced. Table 7 lists the four LCA studies on PHA, for which the results have been reproduced. There are only 6 studies on the LCA of PHA production systems,[18,19,23,31–33] among which, the first 4 studies can be reproduced and validated as they made the inventory data transparently or accurately available. Table 7 shows the material and energy inventory data of the LCA studies reproduced. The differences between the calculated and the published GWP values are explained in Table 7. Also, the calculated GWP accounts for the gate-to-gate systems to keep consistency between the various studies. Owing to a 6 times greater China's electricity mix GWP emission factor and smaller or pilot scale operations, the PHA production systems (Food waste scenarios 1 and 2 (FoodW S1 and FoodW S2)) by Wu *et al.* (2022) have a much greater GWP compared to the other studies.[23] Replacing China's electricity mix emission factor with GB's (Great Britain's) electricity mix emission factor lowers the GWP to less than 10 kg CO_2e per kg. Wastewater large-scale (LS) system (acidogenic fermentation followed by PHA accumulation using volatile fatty acid-fed bacteria) by Vea *et al.* (2021)[31] reported the GWP with all the credits from substitutions. Its gate-to-gate GWP impact exceeds the cradle-to-cradle GWP impact. For a sludge gasification (gas) followed by syngas fermentation scenario by Vogli *et al.* (2020),[18] their published and this paper's reproduced GWP values exactly match. Martin-Gamboa *et al.* (2023)[19] showed another acidogenic fermentation followed by PHA accumulation using a volatile fatty acid-fed bacteria system, for which the reproduced GWP and the reported GWP without the consideration of the credit from the feedstock closely match. These prove that the LCA framework with the selected LCI databases (Table 1) developed in this study largely apply to LCA studies of PHA biosynthesis systems and can be adaptable to other studies.

Applying the LCA framework with the LCI databases in Table 1, LCIA results are generated for the given PHA pro-

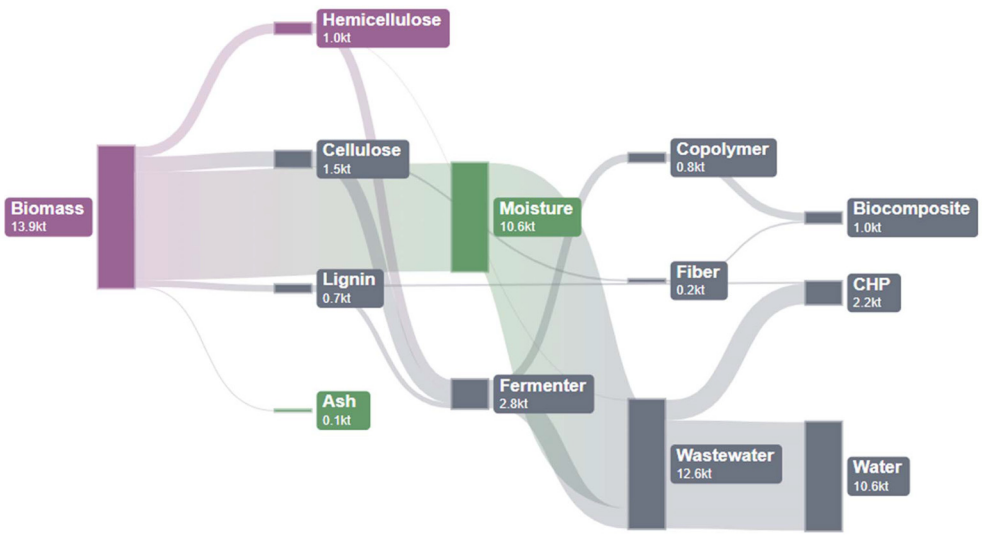

Fig. 5 Material flow analysis from biomass to various outlets.

Table 7 The GWP results were validated, and thereby the life cycle inventory databases for the published studies were validated based on their published inventories

Basis: 1 kg PHA	FoodW S1	FoodW S2	Wastewater LS	Sludge gas	MSW photo	Unit
Sodium hydroxide	0.3325	0.1360			0.4000	kg
Sulfuric acid	0.1151	0.0105				kg
Polydimethylsiloxane (defoamer)	0.0230	0.0010				kg
Trichloromethane (solvent)	0.7304	0.0643				kg
Sodium hypochlorite	1.0696	0.1334	0.19		0.3401	kg
Dimethyl carbonate				0.19		kg
Ammonia			0.3333			kg
Citric acid					0.1050	kg
Lime					0.0123	kg
Surfactant solvent			0.5350			kg
Nitrogen	0.0306					kg
Water	28.4340		8.9243	695.88	0.1143	kg
Electricity	300	101.20	4.78	18.53	4.8	MJ
Heat			2.21	51.33	0.717	MJ
Wastewater treatment	0.26		0.01			m^3
Solid waste	5.23					kg
GWP (calculated with GB electricity mix emission factor unless otherwise stated and without GWP credit from biomass)	69 (with China grid electricity emission factor of 0.83)	60 (with China grid electricity emission factor of 0.83)	3.7 (without GWP credit from biomass, substitution and recycling)	3	2.9	kg CO_2e
GWP (published value with regional electricity mix emission factor and without GWP credit from biomass)	70 (with China grid electricity emission factor of 0.83)	52 (with China grid electricity emission factor of 0.83)	0.76 (including GWP credit from biomass, substitution and recycling)	3	3.5	kg CO_2e
Reference	Wu *et al.* (2022)[23]	Wu *et al.* (2022)[23]	Vea *et al.* (2021)[31]	Vogli *et al.* (2020)[18]	Martin-Gamboa *et al.* (2023)[19]	

duction system. Fig. 6 shows the GWP hotspot or contribution analysis of the various inventories in Table 1. The hotspots are sodium hydroxide, sodium phosphate, and steam. Fig. S3 further emphasizes consistent hotspots across all ReCiPe (M) (H) life cycle impact categories. Fig. 6 also shows the net GWP savings by the PHA biocomposite system from substituting the fossil-based equivalent polypropylene system. The total GWP impact of the PHA production process (Fig. 3) is 1.51 kg CO_2e per kg, which is lower than those reported in the literature (Table 7) as well as the fossil-based equivalent polypropylene

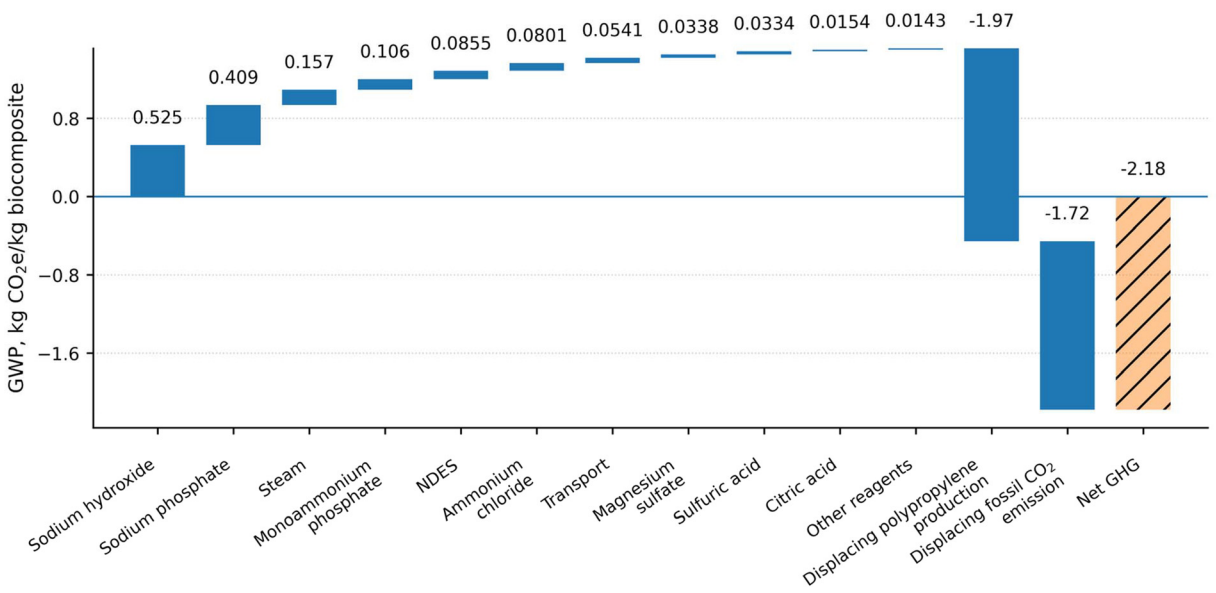

Fig. 6 GWP (kg CO_2e per kg PHA biocomposite) hotspot analysis of inventories and savings from displacing the fossil-based polypropylene cradle-to-grave system by the PHA biocomposite cradle-to-grave system.

cradle-to-gate system, which has a GWP of 1.97 kg CO_2e per kg. Displacing the cradle-to-grave fossil-based equivalent polypropylene system, which additionally emits fossil CO_2 from the embedded carbon in polypropylene: 1.72 kg CO_2e per kg, the cradle-to-grave PHA system would save the GWP by 2.18 kg CO_2e per kg, *i.e.*, by 60% (from 3.69 kg CO_2e per kg GWP of the polypropylene system). This is illustrated by the waterfall plot in Fig. 6. Furthermore, 1.26 GWh of electricity export per 1 ktpa PHA (Table 1) can provide an additional GWP saving of 0.5 kg CO_2e per kg PHA (73% reduction) can be obtained. The current global market for propylene is valued at approximately 126.2 million metric tonnes in 2024. The market is projected to grow to ~155.2 million metric tonnes by 2030, driven by increased demand from the automotive, consumer goods, and electronics industries. Thus, at the 2030 production rate, displacing polypropylene can save GWP by >340 million tonnes CO_2e.

The ReCiPe (M) (H) full impact characterization results of the PHA biocomposite production system are shown in SI (Table S2). A comparison between the PHA biocomposite biosynthesis system, fossil-based equivalent polypropylene system (Ecoinvent 3.10: Polypropylene, granulate {RER}| production | Cut-off) (Table 1), and two equivalent starch-based polyester systems (Ecoinvent 3.10: Polyester-complexed starch biopolymer {RER}| production | Cut-off, and Polyester-complexed starch biopolymer {RoW}| production | Cut-off) shows that the PHA biocomposite system performs better in the overall single score method of ReCiPe (M) (H), as shown in Fig. 7.

Furthermore, a Monte Carlo simulation (over 5000 runs) has been performed to study the effect of the key variables' changes on the GWP impact (Fig. 8). The key variables, *i.e.*, hotspots, sodium hydroxide, sodium phosphate, and steam requirements of the system, are varied by ±10% standard deviation. As a result, the mean, median, standard deviation, coefficient of variance, 2.5% and 97.5% GWP values and standard error mean obtained are: 1.51 kg CO_2e per kg, 1.51 kg CO_2e per kg, ±31.5%, ±20.8%, 0.893 kg CO_2e per kg, 2.15 kg CO_2e per kg, and 0.00446, respectively, using SimaPro 9.6. These statistical terms are explained in Sadhukhan *et al.* (2025)[42] and Luo *et al.* (2025).[48] There is only a 3.7% probability of the GWP of the PHA biocomposite production process exceeding that of fossil-based polypropylene. The Monte Carlo simulation profiles are also shown for the impact categories for which the planetary safe operating boundaries have been transgressed:[42,48] particulate matter, freshwater eutrophication, freshwater ecotoxicity, fossil resource scarcity and water consumption, in Fig. 8. Their coefficient of variance is 26%, 30%, 33%, 16% and 36%, respectively. The fossil resource saving potential estimation is thus the most robust (less uncertain) compared to other categories.

TEA

The mass and energy balance, LCA and TEA models have been made available *via* open-source software with a user-friendly graphical interface: https://clovecircle.com/standalone/PHA-from-lignocellulose-lca-tea.html. It allows users to examine the effects of input variables on the (output) balance, TEA and LCA/GWP results. Table 2 shows the capital cost estimation, including the delivered cost of equipment, following eqn (13). The total capital cost estimated is US$16 million for a 1 ktpa PHA biocomposite production rate (Table 2). The literature reported a total capital cost of US$62–179 million for a 9 ktpa PHA biocomposite production rate (Chavez *et al.*, 2022).[15] By projecting this study's TEA model for a 9 ktpa PHA biocomposite production rate, the total capital cost estimated is US $94 million, which falls within the published range of the total capital cost. Increasing the lang factor to 5.03 [26] increases the total capital cost to US$157 million, which is on the higher range of the published capital cost for 9 ktpa PHA biocomposite production rate. Thus, a lang factor of 3–5 and the parameters in Table 2 are valid. The estimated total capital investment is US$94–157 million, which falls within the published range of the total capital investment of US$62–179 million for a 9 ktpa PHA biocomposite production rate.

Using the price information in Table 3, the annual capital cost, indirect capital cost-dependent fixed operating cost, variable operating cost, miscellaneous operating cost, feedstock cost and product value are calculated using eqn (14)–(21), as shown in Fig. 9.

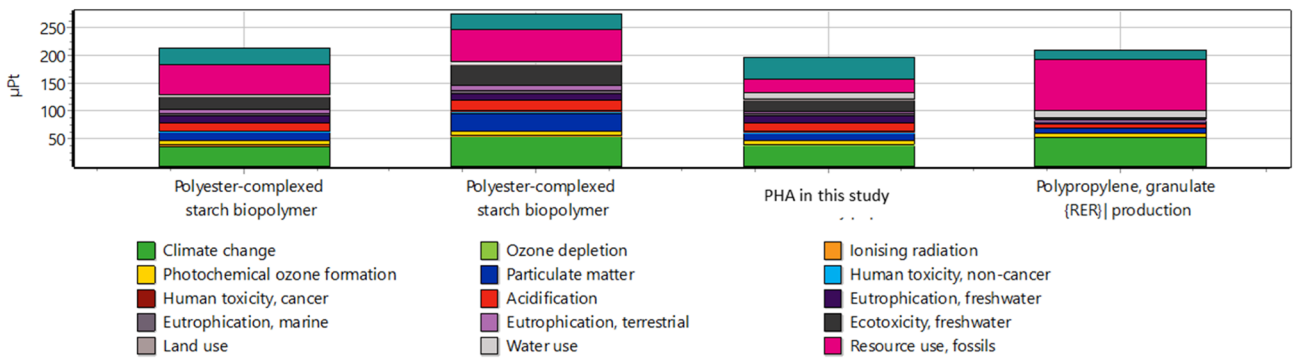

Fig. 7 ReCiPe (M) (H) single score relative comparison between the PHA biocomposite synthesis system, two equivalent polyester systems and the fossil-based equivalent polypropylene system.

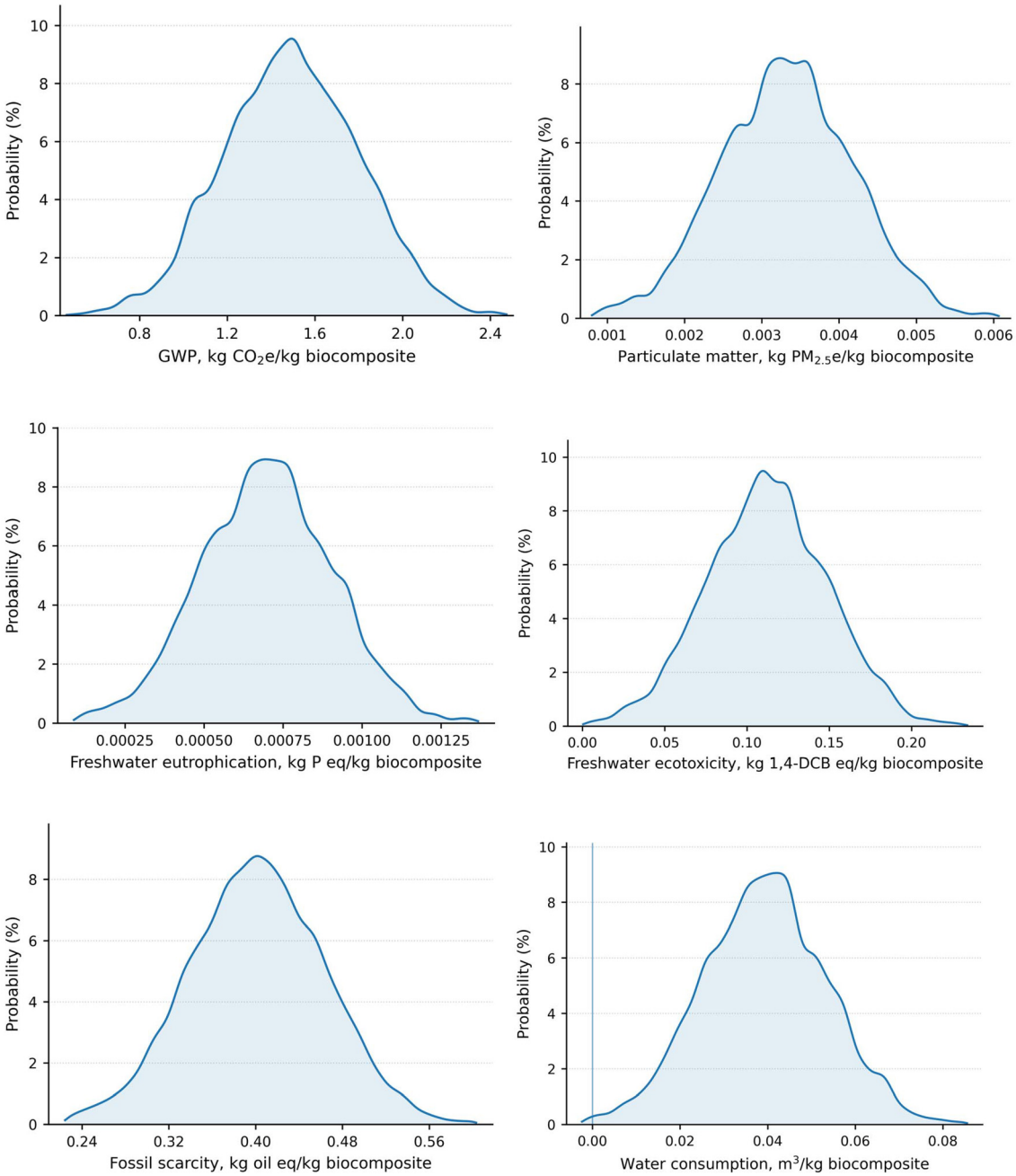

Fig. 8 Monte Carlo simulation of GWP (kg CO_2e per kg PHA biocomposite), particulate matter (kg PM2.5e per kg PHA biocomposite), freshwater eutrophication (kg P e per kg PHA biocomposite), freshwater ecotoxicity (kg 1,4-dichlorobenzene (DCB) e per kg PHA biocomposite), fossil resource scarcity (kg oil e per kg PHA biocomposite) and water consumption (m^3 kg^{-1} PHA biocomposite), due to sodium hydroxide, sodium phosphate, and steam requirements' variations by ±10% standard deviation.

The TEA results in Fig. 9 are compared against a 10 ktpa sucrose-based halophilic PHA manufacturing system.[49] Projecting our TEA model to 10 ktpa PHA biocomposite production gives a total capital investment of 10.2 million US$, comparable to their reported capital cost of US $9.96–10.9 million. The operating cost (Opex) hotspots are feedstock cost, variable Opex, labor cost-dependent fixed Opex, miscellaneous Opex, and indirect cost-dependent fixed Opex, with a contribution of 28%, 27%, 23%, 17% and 5%, respectively. With a slightly varying proportion, the same chronological order can be seen in the recent study.[49] Their reported labor cost of 3.4 million US$ for 10 ktpa capacity,[49] for example, aligns well with the labor cost of 0.28 million US$ for 1 ktpa capacity in this study. Their feedstock and energy costs are three times higher than those in this study because of the use of first-generation feedstock and the lack of on-site energy

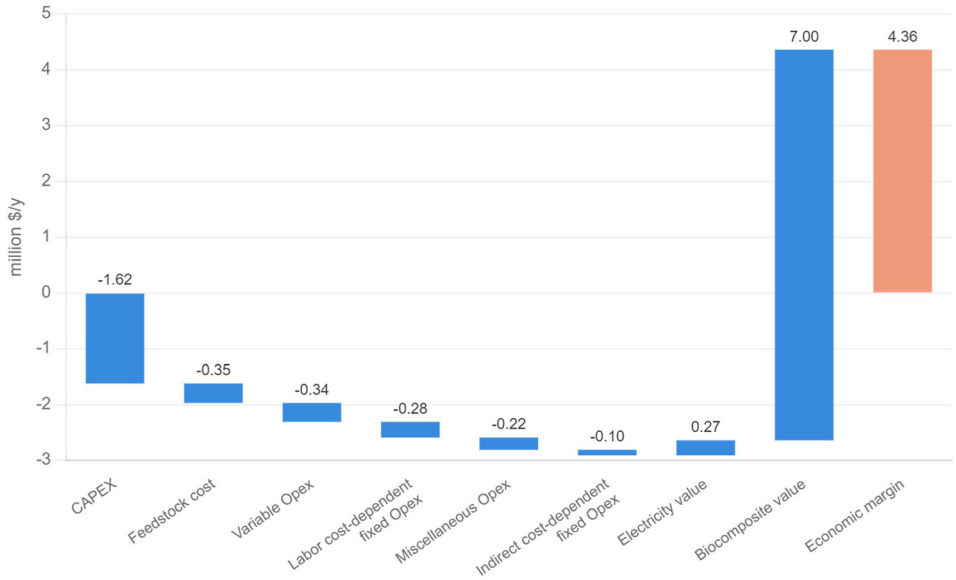

Fig. 9 TEA contribution analysis and annual economic margin of the PHA biocomposite cradle-to-grave system.

generation in their study.[49] Without the on-site electricity generation, this study's operating cost would increase by two-fold, demonstrating the better viability of lignocellulose by diverting excess remaining organics in bioenergy generation to run the plant. In this study, the excess electricity generated, *i.e.*, 4.5 TJ per years (Table 3), gives the plant a revenue of 0.27 million $ per years (Fig. 9).

The NPV profile (eqn (22)) is shown in Fig. 10. The payback time obtained is 5 years and the NPV at the 10th year is 10.67 million US$ for the data given in Tables 2, 3 and for the PHA biocomposite market price of US$7 per kg PHA.[35,48,49] This payback time is close to the observed range by the studies with the waste biomass substrate, *e.g.*, <4 years for 9 ktpa PHA production rate (Leong *et al.*, 2017).[62] The cost of production of PHA biocomposites is US$2.6 per kg (€2.2 per kg or £2 per kg). Thus, this minimum selling price of US$2.6 per kg of PHA biocomposites determines that it can even be sold at its minimum reported market price of $4 per kg.[48,49] The payback time would increase to 7 years for a PHA biocomposite market price of $6 per kg.[48,49] The literature also shows the similar ranges of PHA cost of production, €2.20–5.00 per kg (Martin-Gamboa *et al.*, 2023);[19] US$5.41–6.25 per kg (Wu *et al.*, 2023),[23] US$2.41–4.83 per kg (Rajendran and Han, 2022);[63] US$4–8 per kg (Wang *et al.*, 2021);[64] US$5.77–6.12 per kg (Leong *et al.*, 2017);[62] and US$3.93 per kg (Bengtsson *et al.*, 2017).[65]

A sensitive variable is the PHA biocomposite production capacity, an increase in which lowers its production cost (Fig. 10). Increasing the capacity from 0.3 to 1 ktpa decreases the cost of producing PHA biocomposites from US$3.13 per kg to US$2.6 per kg. The PHA biocomposite production capacity

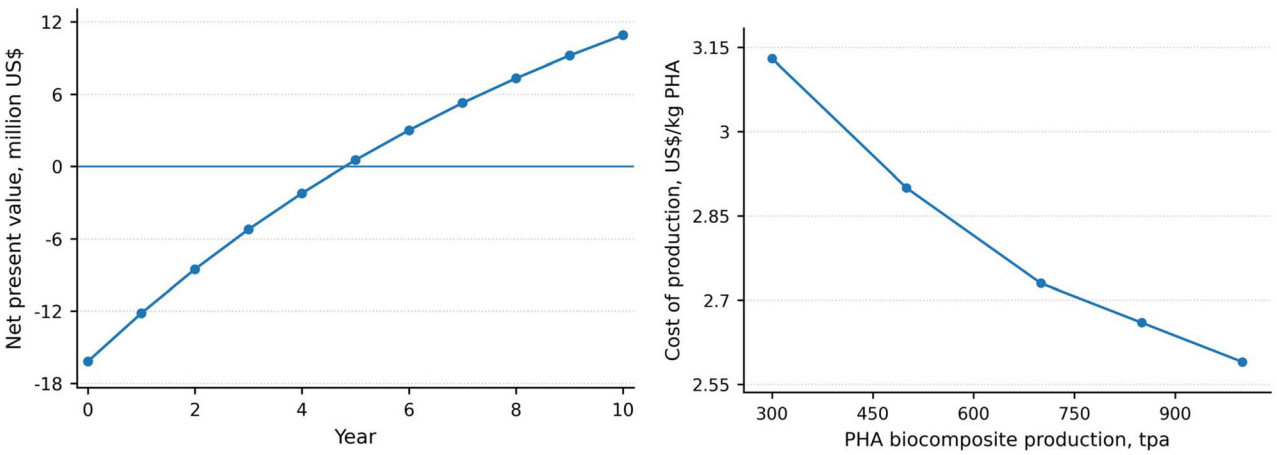

Fig. 10 NPV for the data given in Tables 2 and 3 and for a PHA biocomposite price of US$7 per kg (left) and decreasing cost of production with increasing production capacity of PHA biocomposites (right).

of >0.3 ktpa gives a payback time of <10 years. Below the 0.3 ktpa PHA biocomposite production capacity, NPV is not viable. Thus, iteratively, the functional unit of 1 ktpa of PHA biocomposite production capacity for a sustainable design has been decided as it should be according to the ISO14040-44.

Conclusions

This study establishes an integrated dynamic simulation–life cycle assessment–techno-economic analysis (DS–LCA–TEA) framework for industrial-scale PHA biocomposite production from lignocellulosic residues, enabling internally consistent scale-up from experimentally grounded fermentation dynamics to plant-wide mass/energy balances and sustainability metrics. A DS model has been developed to describe microbial biomass growth, substrate and nitrogen utilization, and PHA accumulation in fed-batch fermentation, based on kinetic mass-balance equations and calibrated against experimental data for *C. necator* grown on cereal waste. Sensitivity analysis identified key kinetic parameters governing cell biomass growth and PHA synthesis, which were subsequently optimized using differential evolution to minimize model-data error. The calibrated model accurately reproduced experimental trends, achieving high Nash–Sutcliffe efficiencies for both cell biomass and PHA, and revealed that maintaining constant substrate and nitrogen concentrations maximizes PHA accumulation (~6.6 g L^{-1} at ~30 h). The results demonstrate that controlled fed-batch operation is critical to prevent PHA re-consumption and provide robust, time-resolved inputs for downstream LCA and TEA. The process is scaled using resulting mass balances from DS, and includes biomass fractionation, fermentation, PHA recovery, composite manufacturing, recycling, and in-process bioenergy/CHP recovery. The LCA has been conducted in accordance with ISO14040-44 to evaluate the cradle-to-grave environmental performance of a circular PHA biocomposite system, using a functional unit of 1 ktpa production and the ReCiPe (M) (H) impact method with a focus on GWP. The inventory flows have been built from validated literature datasets and assigned to Ecoinvent 3.10 background life cycle inventory databases. Results show a 60% GWP saving relative to fossil-based equivalent polypropylene. Hotspot and Monte Carlo uncertainty analyses helped in developing a robust climate-mitigation strategy through in-process material and energy recoveries. The TEA evaluated the commercial feasibility of a 1 ktpa PHA biocomposite plant using standard chemical engineering cost correlations, combining capital expenditure, operating costs, product revenues and discounted cash-flow analysis. Capital costs were estimated *via* scaled equipment costs and Lang factors, yielding a total capital investment of ~US$16 million for 1 ktpa PHA biocomposite manufacturing capacity, consistent with literature when scaled to larger capacities. The system achieves a competitive production cost as low as $2.6 per kg with electricity export, demonstrating that process integration, energy recovery and sufficient production scale are key levers for economic viability.

Author contributions

JS: conceptualization, data curation, formal analysis, funding acquisition, investigation, methodology, project administration, resources, software, supervision, validation, visualization, writing – original draft, and writing – review & editing; XH: data curation, formal analysis, investigation, methodology, resources, software, validation, visualization, writing – original draft, and writing – review & editing; RS: data curation, formal analysis, software, visualization; JBS and KD: visualization, writing – original draft; AB, JJW, CGY and AR: writing – review & editing.

Conflicts of interest

The authors declare no conflict of interest.

Abbreviations

Nomenclature

C_X	Cell biomass concentration, g cell per L
C_P	PHA concentration, g PHA per L
C_S	Substrate concentration, g substrate per L
C_N	Nitrogen concentration, g nitrogen (N) per L
K_S	Saturation constant of substrate, g substrate per L
K_N	Saturation constant of nitrogen, g N per L
K_P	Saturation constant of PHA, g PHA per L
K_{IS}	Inhibition constant of substrate, g substrate per L
K_{IN}	Inhibition constant of nitrogen, g N per L
K_{PS}	Saturation constant for PHA production, g substrate per L
K_{PIS}	Substrate inhibition constants for PHA production, g substrate per L
K_{PIN}	Nitrogen inhibition constants for PHA production, g N per L
C_X^{max}	Maximum active cell biomass concentration, g cell per L
μ_{xs}^{max}	Maximum specific cell biomass growth rate on substrate, g cell per g substrate per h
μ_{xp}^{max}	Maximum specific cell biomass growth rate on PHA, g cell per g PHA per h
M_{ps}^{max}	Maximum specific PHA production rate on substrate, g PHA per g substrate per h
C_{S_F}	Substrate concentration in the given feed method, g L^{-1}
C_{N_F}	Nitrogen concentration in the given feed method, g L^{-1}
ρ_{FS}	Density of substrate in the given feed solution, g L^{-1}
ρ_{FN}	Density of substrate in the given nitrogen solution, g L^{-1}
ρ_w	Density of water, g L^{-1}
$F(t)$	Total feed flowrate, L h^{-1}
$F_S(t)$	Substrate feed flowrate, L h^{-1}
$F_N(t)$	Nitrogen feed flowrate, L h^{-1}
$V(t)$	Bioreactor volume, L
Y_{PS}	PHA yield over substrate, g PHA per g substrate
Y_{XN}	Cell biomass yield due to nitrogen, g cell per g N
Y_{XP}	Cell biomass yield due to PHA, g cell per g PHA

Y_{XS}	Cell biomass yield due to substrate, g cell per g substrate
f_P	PHA-to-cell biomass ratio C_P/C_X
f_P^{max}	Maximum PHA-to-cell biomass ratio
α	Cell density inhibition coefficient
β	Saturation exponent for PHA synthesis

Data availability

The datasets generated and analysed during this study, including dynamic simulation outputs, are available in an open repository, with persistent identifiers to be provided upon acceptance. The dynamic simulation source code and analysis scripts are available *via* a public code repository: the open-source GitHub codes https://github.com/jhumasadhukhan/pha_optimisation/blob/main/dynamicsim.py and https://github.com/nicolehu0306-crypto/Dynamical-modelling-of-PHA-production. TEA and LCA data are available open-source: https://clovecircle.com/standalone/PHA-from-lignocellulose-lca-tea.html.

Supplementary information (SI) is available. See DOI: https://doi.org/10.1039/d6gc00337k.

Acknowledgements

The authors gratefully acknowledge the funding support of BBSRC under grant number BB/Z517100/1 and the National Science Foundation Office of International Science and Engineering (NSF OISE 2435227) for the Global Center for Sustainable Bioproducts https://globalcsb.sites.utk.edu/ that undertook this work. This research was also supported by the Bio&Medical Technology Development Program of the National Research Foundation (NRF), funded by the Korean government (MSIT) (No. RS-2024-00451875). The authors also acknowledge the support of BB/Y008456/1: ELEMENTAL Engineering Biology Mission Hub and EBNet (Environmental Biotechnology Network) BB/S009795/1. The authors gratefully acknowledge the HTML code help of https://github.com/LampOfSocrates/clove-circle/blob/main/standalone/PHA-from-lignocellulose-lca-tea.html in building the software https://clovecircle.com/standalone/PHA-from-lignocellulose-lca-tea.html.

References

1 OECD, 2024. https://www.oecd.org/en/publications/policy-scenarios-for-eliminating-plastic-pollution-by-2040_76400890-en.html accessed January 2026.
2 Fortune Business Insights, 2025. https://www.fortunebusinessinsights.com/plastics-market-102176 accessed January 2026.
3 K. Houssini, J. Li and Q. Tan, *Commun. Earth Environ.*, 2025, **6**(1), 257.
4 BBIA, 2025. https://bbia.org.uk/the-truth-about-bioplastics/ accessed January 2026.
5 IPCC, 2022. https://www.ipcc.ch/report/ar6/wg3/ accessed January 2026.
6 UNCTD, 2024. https://unctad.org/news/countries-agree-300-billion-2035-new-climate-finance-goal-what-next accessed January 2026.
7 Z. Li, J. Yang and X. J. Loh, *NPG Asia Mater.*, 2016, **8**(4), e265.
8 A. S. Mathuriya and J. V. Yakhmi, Polyhydroxyalkanoates: biodegradable plastics and their applications, in *Handbook of Ecomaterials*, Springer, Cham, 2017, pp. 1–29.
9 P. Guerra-Blanco, O. Cortes, T. Poznyak, I. Chairez and E. I. García-Peña, *Eur. Polym. J.*, 2018, **98**, 94–104.
10 M. Koller, *Fermentation*, 2018, **4**(2), 30.
11 M. S. I. Mozumder, L. Goormachtigh, L. Garcia-Gonzalez, H. De Wever and E. I. Volcke, *Bioresour. Technol.*, 2014, **155**, 272–280.
12 J. Sadhukhan, B. G. Pollet and M. Seaman, *Energies*, 2022, **15**(15), 5486.
13 B. Drosg, I. Fritz, F. Gattermayr and L. Silvestrini, *Chem. Biochem. Eng. Q.*, 2015, **29**(2), 145–156.
14 L. Garcia-Gonzalez, M. S. I. Mozumder, M. Dubreuil, E. I. Volcke and H. De Wever, *Catal. Today*, 2015, **257**, 237–245.
15 B. A. Chavez, V. Raghavan and B. Tartakovsky, *RSC Adv.*, 2022, **12**(25), 16105–16118.
16 L. Garcia-Gonzalez and H. De Wever, *Appl. Sci.*, 2018, **8**, 1416.
17 J. Sadhukhan, J. R. Lloyd, K. Scott, G. C. Premier, H. Y. Eileen, T. Curtis and I. M. Head, *Renewable Sustainable Energy Rev.*, 2016, **56**, 116–132.
18 L. Vogli, S. Macrelli, D. Marazza, P. Galletti, C. Torri, C. Samorì and S. Righi, *Energies*, 2020, **13**(11), 2706.
19 M. Martin-Gamboa, L. D. Allegue, D. Puyol, J. A. Melero and J. Dufour, *J. Cleaner Prod.*, 2023, **428**, 139421.
20 M. López-Cuellar, J. Alba-Flores, J. G. Rodríguez and F. Pérez-Guevara, *Int. J. Biol. Macromol.*, 2011, **48**, 74–80.
21 D. Ballard, P. Holmes and P. Senior, in *Recent Advances in Mechanistic and Synthetic Aspects of Polymerization*, Springer, Berlin/Heidelberg, Germany, 1987, pp. 293–314.
22 J. M. Dias, L. S. Serafim, P. C. Lemos, M. A. Reis and R. Oliveira, *Biotechnol. Bioeng.*, 2005, **92**(2), 209–222.
23 M. Wu, X. Gong, X. Liu, W. Tu, P. Yu, Y. Zou and H. Wang, *Environ. Sci. Technol.*, 2022, **57**(3), 1467–1478.
24 K. Dietrich, M. J. Dumont, L. F. Del Rio and V. Orsat, *New Biotechnol.*, 2019, **49**, 161–168.
25 S. Obruca, P. Benesova, L. Marsalek and I. Marova, *Chem. Biochem. Eng. Q.*, 2015, **29**(2), 135–144.
26 J. Sadhukhan, K. S. Ng and E. Martinez-Hernandez, *Biorefineries and Chemical Processes: Design, Integration and Sustainability Analysis*, Wiley, 2014.
27 S. Bellini, F. Demichelis, T. Tommasi, L. Tarraran and D. Fino, *J. Environ. Chem. Eng.*, 2024, **12**(1), 111661.
28 E. G. Kiselev, A. V. Demidenko, N. O. Zhila, E. I. Shishatskaya and T. G. Volova, *Bioengineering*, 2022, **9**(4), 154.
29 M. Shemfe, S. Gadkari, E. Yu, S. Rasul, K. Scott, I. Head, S. Gu and J. Sadhukhan, *Bioresour. Technol.*, 2018, **255**, 39–49.

30 T. Lopez-Arenas, M. González-Contreras, O. Anaya-Reza and M. Sales-Cruz, *Comput. Chem. Eng.*, 2017, **107**, 140–150.
31 E. B. Vea, S. Fabbri, S. Spierling and M. Owsianiak, *Sci. Total Environ.*, 2021, **788**, 147544.
32 S. Lee, I. Lee, D. Seo, H. Kim, G. Joo, S. Lee and K. Park, *ACS Sustainable Chem. Eng.*, 2023, **12**(1), 72–84.
33 M. S. del Oso, M. Mauricio-Iglesias, A. Hospido and B. Steubing, *J. Cleaner Prod.*, 2023, **383**, 135331.
34 EUP Egypt, 2025. https://eupegypt.com/blog/pha-plastic-polyhydroxyalkanoates/ accessed January 2026.
35 Helian Polymers, 2025. https://helianpolymers.com/ accessed January 2026.
36 F. Lin, X. Chen and H. Yao, *J. Hydrol. Eng.*, 2017, **22**(11), 05017023.
37 J. Sadhukhan, S. Gadkari, E. Martinez-Hernandez, K. S. Ng, M. Shemfe, E. Torres-Garcia and J. Lynch, *Green Chem.*, 2019, **21**(10), 2635–2655.
38 Y. K. Wan, J. Sadhukhan and D. K. Ng, *Chem. Eng. Res. Des.*, 2016, **107**, 102–116.
39 D. Humbird, R. Davis, L. Tao, C. Kinchin, D. Hsu, A. Aden, P. Schoen, J. Lukas, B. Olthof, M. Worley, D. Sexton and D. Dudgeon, Process design and economics for biochemical conversion of lignocellulosic biomass to ethanol: Dilute-acid pre-treatment and enzymatic hydrolysis of corn stover, National Renewable Energy Laboratory (NREL), Technical report, 2011, NREL/TP-5100-47764.
40 DSMZ, 2011, https://www.dsmz.de/microorganisms/medium/pdf/DSMZ_Medium81.pdf accessed January 2026.
41 House of Commons, 2024, https://commonslibrary.parliament.uk/research-briefings/cbp-8515/ accessed January 2026.
42 J. Sadhukhan, O. J. Fisher, B. Cummings and J. Xuan, *J. CO2 Util.*, 2025, **92**, 103013.
43 E. Martinez-Hernandez, J. Sadhukhan, J. Aburto, M. A. Amezcua-Allieri, S. Morse and R. Murphy, *Clean Technol. Environ. Policy*, 2022, **24**(6), 1709–1725.
44 J. Sadhukhan, S. Sen and S. Gadkari, *J. Cleaner Prod.*, 2021, **309**, 127457.
45 J. Sadhukhan, *Appl. Energy*, 2014, **122**, 196–206.
46 J. Sadhukhan, K. S. Ng, N. Shah and H. J. Simons, *Energy Fuels*, 2009, **23**(10), 5106–5120.
47 J. Sadhukhan, *Renewable Energy*, 2022, **184**, 960–974.
48 H. Luo, D. Yang, J. Sadhukhan, V. Costica, R. Dorey, Q. Song and M. M. Titirici, *ChemSusChem*, 2025, e202500503.
49 J. Sadhukhan, S. Gadkari and R. I. Muazu, Technoeconomic analysis and life cycle assessment methodologies for microbial electrochemical systems, in *Material-Microbes Interactions*, Academic Press, 2023, pp. 409–423.
50 https://www.mordorintelligence.com/industry-reports/poly-hydroxyalkanoate-market accessed January 2026.
51 I. Levett, X. Bai, P. Lant, B. Laycock, M. Brunner and S. Pratt, *Bioresour. Technol.*, 2026, **445**, 134078.
52 Business Analytiq, 2025, https://businessanalytiq.com/procurementanalytics/index/sodium-hydroxide-price-index/ accessed January 2026.
53 Ofgem, 2025, https://www.ofgem.gov.uk/information-consumers/energy-advice-households/energy-price-cap-explained accessed January 2026.
54 M. Langholtz, M. Davis, L. Eaton, M. Hilliard, C. Brandt, E. Webb, C. Hellwinckel, N. Samu, D. Hartley and D. Jones, *Biofuels, Bioprod. Biorefin.*, 2022, **16**(1), 204–218.
55 J. H. Lee, H. C. Lim and J. Hong, *J. Biotechnol.*, 1997, **55**, 135–50.
56 P. R. Patnaik, *Bioresour. Technol.*, 2006, **97**, 1994–2001.
57 G. Du, J. Chen, J. Yu and S. Lun, *Process Biochem.*, 2001, **37**, 219–227.
58 N. Tanadchangsaeng and J. Yu, *Biotechnol. Bioeng.*, 2012, **109**, 2808–2818.
59 P. Cougnon, D. Dochain, M. Guay and M. Perrier, *J. Process Control*, 2011, **21**, 1526–1532.
60 D. Frigon, G. Muyzer, M. C. M. van Loosdrecht and L. Raskin, *Appl. Environ. Microbiol.*, 2006, **72**, 2322–2330.
61 A. Mulchandani and J. H. T. Luong, *Enzyme Microb. Technol.*, 1989, **11**, 66–73.
62 Y. K. Leong, P. L. Show, J. C. W. Lan, H. S. Loh, H. L. Lam and T. C. Ling, *Clean Technol. Environ. Policy*, 2017, **19**(7), 1941–1953.
63 N. Rajendran and J. Han, *Bioresour. Technol.*, 2022, **348**, 126796.
64 K. Wang, A. M. Hobby, Y. Chen, A. Chio, B. M. Jenkins and R. Zhang, *Processes*, 2021, **10**(1), 17.
65 S. Bengtsson, A. Werker, C. Visser and L. Korving, *PHARIO: stepping stone to a sustainable value chain for PHA bioplastic using municipal activated sludge*, Stichting Toegepast Onderzoek Waterbeheer, Amersfoort, The Netherlands, 2017, pp. 1–93.